Mechanical Design and Simulation Studies of A Quadruped Robot Motion Control System

by

Xiang Sheng
B.Sc., Harbin Institute of Technology, 2013

A Thesis Submitted in Partial Fulfillment of the
Requirements for the Degree of

MASTER OF APPLIED SCIENCE

in the Department of Mechanical Engineering

Mechanical Design and Simulation Studies of A Quadruped Robot Motion Control System

by

Xiang Sheng
B.Sc., Harbin Institute of Technology, 2013

Supervisory Committee

Dr. Yang Shi, Supervisor
(Department of Mechanical Engineering)

Dr. Ben Nadler, Departmental Member
(Department of Mechanical Engineering)

Supervisory Committee

Dr. Yang Shi, Supervisor
(Department of Mechanical Engineering)

Dr. Ben Nadler, Departmental Member
(Department of Mechanical Engineering)

ABSTRACT

This thesis focuses on mechanical design and simulation studies of a quadruped robot motion control system, targeting at designing an autonomous legged robot. The designed quadruped robot with "X"-configuration is developed for traversing rocky and sloped terrain with a static walking gait.

The mechanical design of the quadruped robot is illustrated in Chapter 2, including the main body design, leg design and component selection. In the design process, appropriate mechanical structures are utilized to minimize the energy consumption. To improve energy efficiency, a set of principles is proposed. Corresponding implementations are also concretely introduced in this chapter. In addition, to simplify the mechanical structure of the quadruped robot, the mass is symmetrically distributed about the frontal and lateral planes. To improve the leg agility, the leg mass is minimized. On the one hand, the lightweight design is implemented by optimizing the mass distribution of the leg mechanism. On the other hand, the key components are assembled in the body part instead of the legs as many as possible. A sufficient leg length is also selected not only to allow the robot to step on or over obstacles, but also to avoid the leg getting caught by objects. Particularly, the leg structure is demonstrated, including the hip joint, thigh part, knee joint and limb part with a telescoping joint. When the robot sustains extensive payload, the deformed shape in joints may lead to structural failures, thereby influencing the quadrupedal locomotion. Finite element analysis (FEA) is performed when designing the structural components in reasonable structures. The design processes of the shoulder part and brass rod are demonstrated as examples. Based on the setup of loads and fixtures, the maximum

deformed shape of these structural components are analyzed. From FEA simulation results, the yield strength is two orders of magnitude larger than the maximum of von Mises stress. Hence, these components are suitable to be incorporated in the quadruped robot.

Based on the designed mechanical structure, simulation studies of the quadruped robot motion control system are analyzed in Chapter 3, including the modeling for a robotic leg and animated simulation. Since the quadrupedal locomotion is executed by manipulating the postures of four legs, the leg model is significant to the motion control system, thereby being analyzed mathematically. Two links kinematic conversion is implemented between the foot-end trajectory and joint angles. The dynamic model of the leg is also computed to discovery the relationship between the actuating torques and joint angles. To animate the quadrupedal locomotion, a CAD robot model is converted into MATLAB. Following the predefined footfall pattern, four legs move in sequence to execute the creeping gait. The segment of the desired trajectory of the foot-end fits a fifth order polynomial and does not include the set of singular configurations. Then, the PD control is utilized to adjust the leg posture to track the desired path. Furthermore, the actual joint angles are calculated in the MATLAB/SimMechanics quadruped robot by using Euler-Lagrange equations. Lastly, simulation results are presented to analyze the tracking performance in the joint angles and foot-ends.

Finally, conclusions of the thesis are summarized, and future work is presented in Chapter 4.

Contents

List of Tables

List of Figures

ACKNOWLEDGEMENTS

Firstly, I would like to show my sincerest gratitude to my supervisor, Dr. Yang Shi, a decent and professional scholar. It is my honor to be a member of his research group. He provided insightful guidance for my academic research and my personal life. He provided insightful guidance, not only for my academic research, but also in the aspects of personal life. He shared many tips and gave me advice in the individual meetings and group meetings. He also is my role model to teach me how to handle problems in a professional attitude. When I encountered problems, he encouraged me with great enthusiasm, impressive kindness and extraordinary patience. I really appreciate Dr. Yang Shi for providing me the opportunity to initiate my MASc study in Canada.

I would like also to thank committee members, Dr. Ben Nadler and Dr. Hong-Chuang Yang, for their constructive comments.

Moreover, I really enjoy to work with my group members in the Applied Control and Information Processing Lab at the University of Victoria. I want to show my gratitude to the senior students, Dr. Mingxin Liu, Dr. Bingxian Mu, Dr. Chao Shen, Dr. Yuanye Chen, Jicheng Chen, and Kunwu Zhang. They not only helped me countless times to solve academic problems during my research, but also offered the help in life aspect. They helped me in adapting to the new study environment. In addition, I want to thank current students, Qi Sun, Qian Zhang, Henglai Wei, Tianyu Tan, Huaiyuan Sheng, Haoqiang Ji, Zhang Zhang, Chonghan Ma, Chen Ma, Zhuo Li, Tingting Yu, Changxin Liu and Bo Cai for the happy and joyful time that we have spent on Vancouver Island.

Last but not least, I would like to thank my parents for their help and support.

Acronyms

PC	personal computer
DOF	degrees of freedom
PAM	pneumatic artificial muscle
PPAM	pleated pneumatic artificial muscle
WSM	wide stability margin
CPG	central pattern generator
SLIP	spring loaded inverted pendulum
IMU	inertial measurement unit
IEPF	iterative-end-point-fit
MPC	model-predictive control
CAD	computer-aided design
PCB	printed circuit board
PD	proportional-derivative
RISC	reduced instruction set computing
ARM	advanced RISC machine
FPGA	field-programmable gate array
RPM	revolutions per minute
FEA	finite element analysis
LH	left-hind
LF	left-front
RH	right-hind
RF	right-front
COM	center of mass
ESC	electronic speed control

Chapter 1

Introduction

Mobile robots have been developed to replace human beings to work in some complex and dangerous environments, such as humanitarian de-mining, disaster sites, and battlefields. For example, since increasing number of landmines have been deployed, the detection and removal of antipersonnel landmines draw a wide range of concerns. To clear the mines in an area efficiently and safely, the robot is required to be equipped with sensitive sensors, efficient manipulators and advanced mobility functions [16]. The integrated robotic system is built based on a legged robot combining with a sensor for the landmine detection, a manipulator to adjust the position of the sensor, a global-position system to identify the landmine location. To accomplish these tasks, legged robots exhibit potential advantages as follows:

- With solid footholds, legged robots reduce the possibility of stepping on an antipersonnel mine.
- The inherent omnidirectionality of legged robots can steer the direction of movement without forward/backward manoeuvers.
- Legged robots can step over loose and sandy terrain. Equipped with appropriate tactile sensors, legged robots can identify the inclination angle of the contact surface to prevent slippage.
- Legged robot can optimize the posture for the scanning manipulator to approach landmines without changing its footholds.

Based on a legged robot with a hexapod configuration, the "DYLEMA" system is developed to detect and locate landmines [16]. DYLEMA is a Spanish acronym which

means efficient detection and location of antipersonnel landmines. This hexapod platform can realize the locomotion in a relatively high speed. Meanwhile, the robot can maintain stability when three feet alternately provide supports. In addition, a remote operator controls the scanning manipulator through the teleoperation and collaborative control strategies. By adjusting the position of the sensor head and the posture of the scan manipulator, "DYLEMA" can approach the landmines in an appropriate trajectory over terrain irregularities.

Normally, mobile robots can be classified into air robots [17], underwater robots [18] and ground robots [19]. Generally, ground robots can be subdivided into tracked robots, wheeled robots and legged robots [20]. As illustrated in [21], half of land surface cannot be exploited by tracked robots and wheeled robots, but most of the terrain is accessible to legged robots. Additionally, since the path of legged robots is decoupled from the sequence of the footholds, the trajectory pattern is produced [22]. Legged locomotion shows the outstanding performance in various kinds of soil conditions [23] and obstacle avoidance [21]. Compared with wheeled and tracked robots, legged robots present high efficiency in maintaining static balance with a range of choices for footholds [24].

Lots of legged robots have been developed, inspired by the biological feature of wild animals. By applying a reasonable mechanical structure and an appropriate control strategy, legged robots are capable of moving on irregular terrain. Since most of wild animals have the symmetric structure, legged robots usually have an even number of legs [25]. This characteristic can help legged robots to realize efficient gaits and stable locomotion [26]. Based on the number of legs [27], legged robots can be classified into three categories:

- Biped robots with two legs [28],
- Quadruped robots with four legs [29],
- Insectoid robots with more than four legs [30].

Among these categories, quadruped robots are superior to biped robots on aspects of the static stability. Also, compared with insectoid robots, the design and manufacture of quadruped robots are relatively easier due to the simple mechanical structure. To find a compromise leg number for legged robots, following factors are taken into consideration. On the one hand, reducing the leg number can simplify the mechanical structure and control strategy. On the other hand, the stability of the

alternative stepping motion is generally maintained by keeping the projected center of mass (COM) within a polygon, which is formed by the stance legs. The legged robot can keep the balance easier in the locomotion, when using more stance legs alternatively to provide the support. Hence, it is a reasonable compromise to apply four legs in one robot. By choosing alternatively three legs on the ground as the support pattern, the quadruped robot can be a stable and active platform to fulfill highly dynamic tasks, such as mild running turns and jumping over obstacles.

1.1 Configurations of the Quadruped Robot

A reasonable mechanical structure plays a significant role to accomplish various tasks. Robots with different structures are adept at a diverse set of gaits, such as trotting, bounding, and galloping. Since there are few mature quadruped products, it is hard to define a standard mechanical structure of a versatile quadruped robot. Despite the fact that lots of novel mechanisms have been designed, most of them are developed to suit the designated condition. For example, the structure of the flexor reflex is not suitable for the de-mining robot. When the flexor reflex is activated by obstacles, the movement of the foot-end may detonate the mine and lead to an explosion. To avoid the accident, the foot-end of the de-mining robot is designed as a narrow base. Hence, the narrow connecting area can significantly reduce the possibility of the detonation, when the foot-end strikes the ground.

In addition, apart from wild animals, the designers can also absorb the inspiration from typical quadruped robots. As one of the pioneers in robotics research, Boston Dynamics Inc. has developed advanced robots with remarkable performances, in terms of mobility, agility, dexterity and speed. This section introduces several products which are developed by this group, such as “Cheetah I”, “BigDog”, “LittleDog” and “LS3”.

Following the posture classification of “StarlETH” in [1], quadruped robots are divided into the “X”-configuration, “O”-configuration and “M”-configuration. As illustrated in Figure 1.1, when the orientations of the knee joints are towards inside and outside, the postures correspond to the “X”-configuration and “O”-configuration, respectively. When the orientations of the knee joints are towards the same direction, the posture is named as the “M”-configuration. Quadruped robots with different configurations are appropriate for various kinds of tasks. Quadruped robots with the “X”-configuration are adept at static gaits on rough terrain locomotion, such as

"LittleDog" [31]. Generally, quadruped robots with the "O"-configuration specialize in carrying considerable payload, such as "LS3" [32]. Quadruped robots with the "M"-configuration can perform highly dynamic tasks like running and jumping, such as "Cheetah II" [7]. These configurations are extensively implemented in the mechanical design of quadruped robots. The features of different configurations are illustrated by comparing typical quadruped robots below.

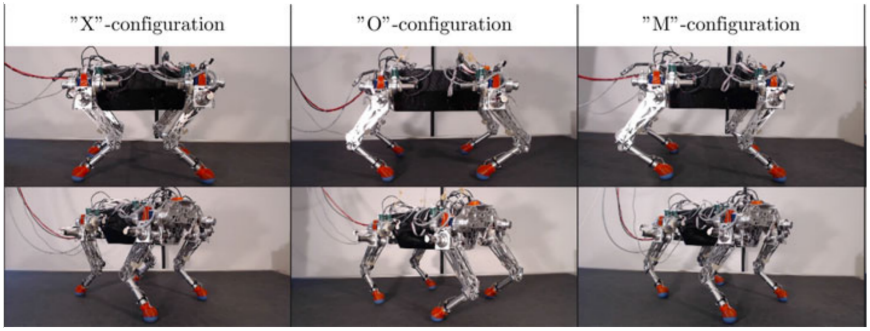

Figure 1.1: Different configurations shown by "StarlETH" [1].

1.1.1 *"M"-configuration*

"Cheetah" series are typical sample robots with the "M"-configuration. As shown in Figure 1.2a. "Cheetah I" (or called "WildCat") is the fastest free running quadruped robot in the world. The robot can run up to 9 m/s while maintaining its balance [2]. The outstanding running speed largely attributes to its articulated back which can flex back and forth on each step. Since the elastic structure is implemented in the body part like some mammals, its running speed can be considerably increased by extending the stride length. Moreover, by upgrading the running controller of the first generation, "Cheetah II" (see Figure 1.2b) can execute mild running turns and jumps over obstacles autonomously [3]. Besides, by minimizing the vertical movements of the body part, "Cheetah II" can also balance objects on its back even running on rough terrain.

Hiroshi Kimura *et al.* from Tokyo Institute of Technology developed "Patrush II" in 1994, as shown in Figure 1.3a. Each leg is actuated by three DC motors with neural oscillation central pattern generator (CPG). By applying the biological-type control, "Patruch II" can perform dynamic walking and present adaptive ability on irregular terrain.

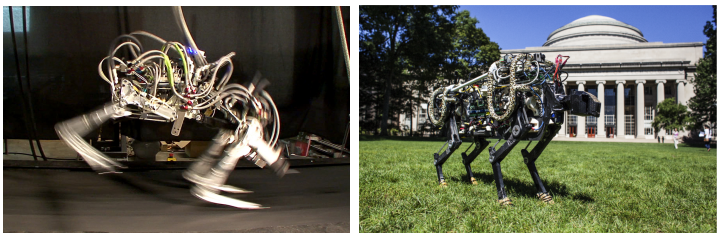

(a) (b)

Figure 1.2: Illustrations of "Cheetah" series with the "M"-configuration: (a) "Cheetah I" [2] and (b) "Cheetah II" [3].

In addition, "Tekken I" with the "M"-configuration was developed around 2000 by Hiroshi Kimura *et al.*. "Tekken I" (see Figure 1.3b) is controlled by a personal computer (PC) and is actuated by Switzerland Maxon DC motors. Each joint is equipped with a photoelectric encoder, a gyroscope, an inclinometer and a tactile sensor. The leg model is controlled by the neural oscillation CPG and a reflection mechanism control system. Particularly, CPG generates the rhythmic motion, while reflection mechanism gains the feedback from the sensor to change the step cycle and phases of CPG. With the feedback information, this robot can walk not only on the ground with pebbles and grasses, but also on hollows and slippery surfaces [13, 33].

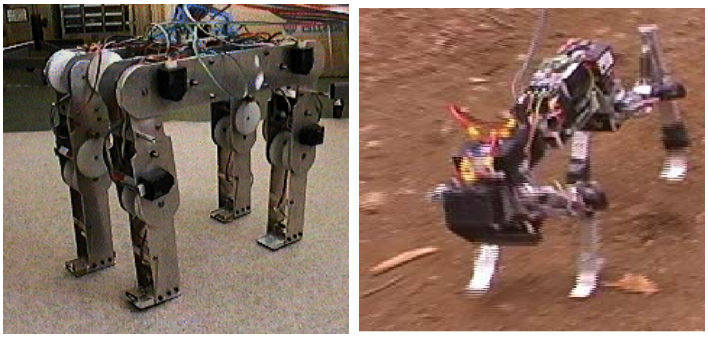

(a) (b)

Figure 1.3: Illustrations of quadruped robots with the "M"-configuration by Hiroshi Kimura *et al.*: (a) "Patrush I" [4] and (b) "Tekken I" [5].

1.1.2 *"X"-configuration*

Quadruped robots with the "X"-configuration can efficiently walk on rough terrain, and even are capable of climbing in some circumstances. As two typical robots with the "X"-configuration, "BigDog" [34] and "LittleDog", which are developed by Boston

Dynamics Inc. in 2005 and 2013 respectively, perform excellent locomotion on rough terrain. "BigDog" is appropriate for a relatively smooth surface with dynamic gaits, and "LittleDog" presents outstanding performance on rough terrain with static gaits.

As shown in Figure 1.4a., "BigDog" is a self-contained quadruped robot, and can execute dynamic walking in the outdoor environment while carrying heavy loads. Four articulated legs are incorporated into "BigDog" to absorb shock and to recycle energy. The four-DOF leg has three active joints and one passive joint, which are built by hydraulic cylinders and a pneumatic spring, respectively. This robotic platform has successfully performed different kinds of locomotion gaits, such as walking, trotting, and bounding. Equipped with a gasoline engine and hydraulic actuators, the robot can carry up to 154 kg payload and last for around 2.5 hours. The power supply is provided by an internal combustion engine to drive a hydraulic pump, which delivers the hydraulic oil to the actuators.

Also, Boston Dynamics Inc. developed "LittleDog" which can traverse a variety of rough terrain quickly and robustly [31], as shown in Figure 1.4b. "LittleDog" is designed for research on learning locomotion by applying motor learning, dynamic control and terrain estimation. For each leg of "LittleDog", two motors are used to actuate the hip joint and one motor is utilized to drive the knee joint with an 85:1 ratio. The mass of the body is much larger than the compliant leg, which are 1.8 kg and 0.25 kg, respectively. "LittleDog" is equipped with a variety of sensors including an IMU, 3-axis force sensors, a high-resolution camera, and so on. Besides, six degrees of freedom (DOFs) position information is provided by a Vicon motion capture environment, which is operated for the quadrupedal locomotion. With the help of a sub-millimeter accuracy terrain map, desired trajectories are computed by an embedded 1 kHz microprocessor, in which an internal proportional-derivative (PD) controller is programmed. In addition, an external computer transmits other control commands through a wireless connection.

1.1.3 *"O"-configuration*

As a typical robot with the "O"-configuration, Legged Squad Support System ("LS3") quadruped robot (see Figure 1.4c) has potential capability in delivering extensive loads.

"LS3" is designed as a rough-terrain robot to help marines and soldiers to carry their load in the battlefield [32]. An "LS3" can carry up to 181 kg of load for a mission

(a) (b) (c)

Figure 1.4: Illustrations of quadruped robots by Boston Dynamics Inc: (a) “BigDog ”, (b) “LittleDog” and (c) “LS3” [2].

covering a 32 km and lasting for 24 hours. By obtaining terrain mapping from stereo and LIDAR sensors, “LS3” can perform autonomous navigation without a dedicated operator, by using terrain sensors and GPS to identify designated locations. “LS3” can keep its paces in uneven and slippery surfaces and can stand upright in spite of some external disturbances.

1.2 Leg Mechanism of the Quadruped Robot

Since the quadrupedal locomotion is executed by controlling the movement of four robotic legs, the leg mechanism plays an essential part of the whole quadruped structure. A multi-degree-of-freedom robotic leg is supposed to incorporate a light-weight construction, low impedance transmission and high torque density motors. A force sensor is usually assembled in the foot-end to measure the direction of contact. Also, by using cameras and various sensors, the locomotion can be controlled by the behaviour generation module, behaviour control module, and low-level joint controller. The leg should be carefully designed in several perspectives, such as increasing the height of center of gravity of the leg and narrowing the volume of the foot-end. The design objectives of a quadruped robot are to perform highly dynamic tasks and to execute rough terrain locomotion.

Generally, the robotic leg implements three types of leg mechanisms, including the compressed air, steel coil springs and compliant mechanisms in [35]. Since the latest one is not implemented in the designed quadruped robot, this mechanism is briefly introduced at the end of this subsection. Furthermore, the leg mechanism can also be classified into linear joints and articulated joints, according the leg configuration. The features of leg mechanisms are illustrated below for each category.

1.2.1 Robotic Legs with Compressed Air

To increase the energy transformation ratio, the inherent compliant behavior of pneumatic actuators can be used to realize mutual transformation of kinetic energy and potential energy. A considerable energy capacity can be generated by compressing air in a container which is made of steel, fiberglass and rubber in tension. The high specific strength can be generated by two common compressed air structures, which are the pneumatic cylinder and pneumatic artificial muscles (PAMs). From the biological perspective, this mechanisms play a role of the muscle which is composed of elastic tendons.

3D One-legged Hopping Machine (linear joints) As a hopping and running robot with a pneumatic cylinder [22], the three dimensional (3D) one-legged hopping machine is designed by Raibert *et al.* in 1986. This robot incorporates a linear telescoping joint to adjust the leg length with hydraulic actuators and air springs. The 3D one-legged hopping machine consists of a body and a compliant leg, as shown in Figure 1.5a [6]. The body comprises actuators, valves and other electronic equipments. The compliant leg is actuated by a pneumatic cylinder. For the pneumatic cylinder, a rubber cushion and linear potentiometer are assembled at the bottom and top, respectively. The compliant leg can minimize the energy consumption in continuous hopping by applying the internal energetic conversion. In addition, the control system regulates the pressure of the lower chamber by changing the air capacity. The upper chamber acts as a passive spring, and connects a pressure regulator with a check valve, as shown in Figure 1.5b [6]. The hopping motion is triggered by controlling the air capacity in the lower chamber. In the stance phase, the low chamber exhausts the air to provide a thrust. The thrust is maximized by activating quick-exhaust values. The spring-mass oscillator is controlled by charging and exhausting the air to adjust the pressure. Without external support, the robot can hop at a speed up to 2.2 m/s.

By controlling the air capacity, the pneumatic cylinder can adjust the leg stiffness in the swing phase. From lots of experimental results, the high pressure can increase the stiffness of spring and reduce the duration of the stance phase. In this way, the robot can hop in a relatively high speed.

Biped "Lucy" and "Mowgli" (articulated joints) As two typical types of PAMs, pleated pneumatic artificial muscles (PPAMs) and Mckibben PAMs are utilized in the biped "Lucy" and "Mowgli", respectively.

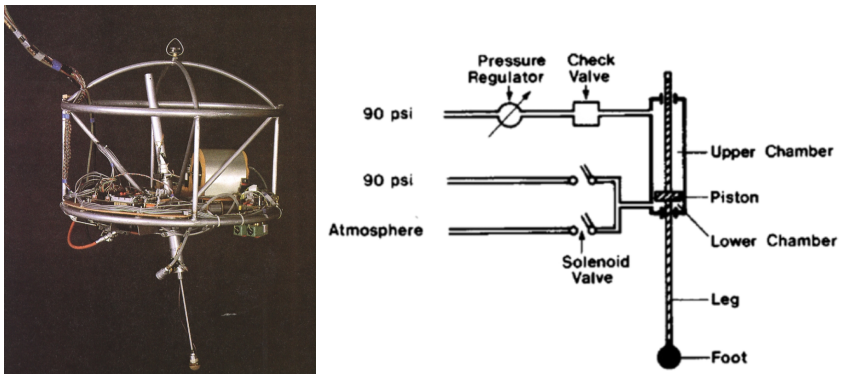

(a) (b)

Figure 1.5: (a) 3D one-legged hopping machine and (b) its pneumatic circuit [6].

The biped "Lucy" has been developed as a six-DOF biped robot which is actuated by twelve PPAMs. As shown in Figure 1.6a, the upper body and two compliant legs are connected by two one-dimensional pin joints [7], which can avoid legs turning over in the frontal plane. Since the PPAM can only be pulled, each articulated joint of the biped "Lucy" is actuated by a pair of PPAMs (see Figure 1.6b) as a bidirectionally working revolute joint. Unlike the pneumatic cylinder, the joint angles and the leg stiffness are controlled independently, and are measured by different gauge pressures separately. By switching the valve, the control strategy is implemented by a one-DOF pendulum, as illustrated in Figure 1.6c.

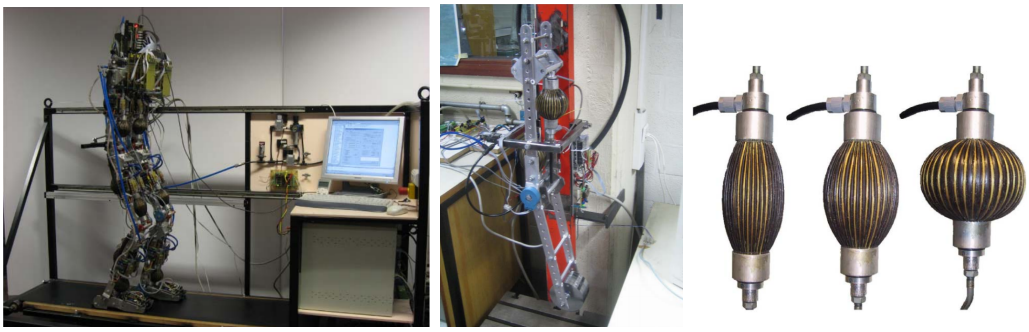

(a) (b) (c)

Figure 1.6: (a) The biped "Lucy" on treadmill, (b) its physical pendulum and (c) 3 contraction levels of the PPAM [7].

Besides, a jumping robot named "Mowgli" has been constructed with the McKibben pneumatic muscle, as shown in Figure 1.7. Six McKibben PAMs are incorporated into two articulated legs to actuate hip, knee and ankle joints. However, unlike

the biped "Lucy", the artificial muscles of "Mowgli" are composed of rubber tubes. For the electro-pneumatic system, "Mowgli" has the potentiometer, pressure sensor and touch switch, which are assembled on the joint, muscle and foot-end, respectively. With 3 kg weight, "Mowgli" can jump up to 0.5 m with soft landings, which is more than 50% of its body height (0.9 m with legs extended).

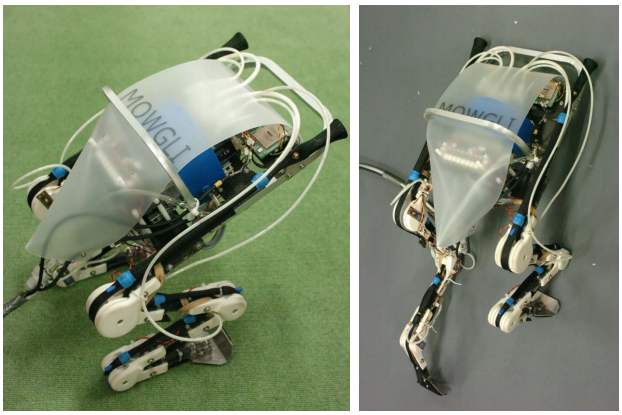

(a) (b)

Figure 1.7: Illustration of "Mowgli": (a) the jumping posture and (b) landing posture [8].

1.2.2 Compliant Legs with Steel Coil Springs

As a popular mechanical structure, steel coil springs are widely incorporated in compliant legs. Several legged robots apply this mechanism at hip joints, such as the ARL "Monopod" and "KOLT".

ARL "Monopod" (linear joints) The Ambulatory Robotics Lab (ARL) "Monopod" is developed by Buehler *et al.*, which is incorporated with the mechanical structure of the pneumatic cylinder and steel coil springs. As shown in Figure 1.8a, the ARL "Monopod" consists of a body and a prismatic leg [9]. The motor torque is converted into an axial force by a timing belt and pulley, as shown in Figure 1.8b. The pitch motion of the body is determined by the leg swing. The 55 Nm hip torque is actuated by an 80 W motor and is transmitted to the joint by a 30:1 gear ratio.

From experimental results, the ARL "Monopod" can move at a speed of 1.2 m/s. By including the leg spring in the leg mechanism, the hip swing motion minimizes the energy consumption with the design. The ARL "Monopod" performs the stable locomotion, including the leg swing phase and vertical hopping motion.

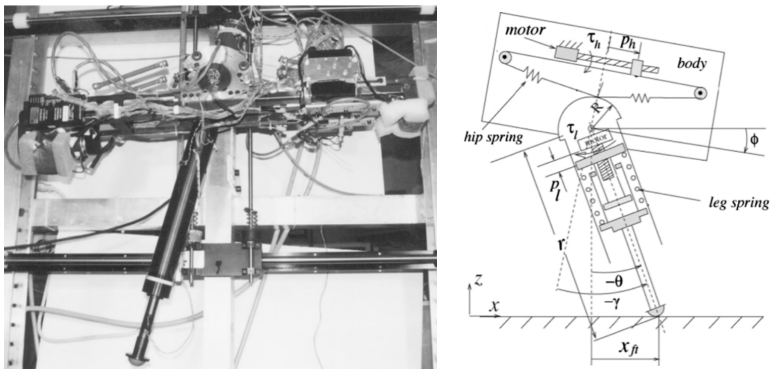

(a) (b)

Figure 1.8: (a) The ARL "Monopod" and (b) the schematic of its important variables [9].

"KOLT" (articulated joints) The Kinetically Ordered Locomotion Test ("KOLT") robot (see Figure 1.9a) is developed to perform the galloping gait by Ohio State University and Stanford University [36].

Inspired by the biological feature of the goat leg, the electro-pneumatic leg of "KOLT" comprises the body, thigh, shank and coil springs [10]. To decrease the impact force at collision, the compliant leg applies the pneumatic cylinder with low inertia, as shown in Figure 1.9b.

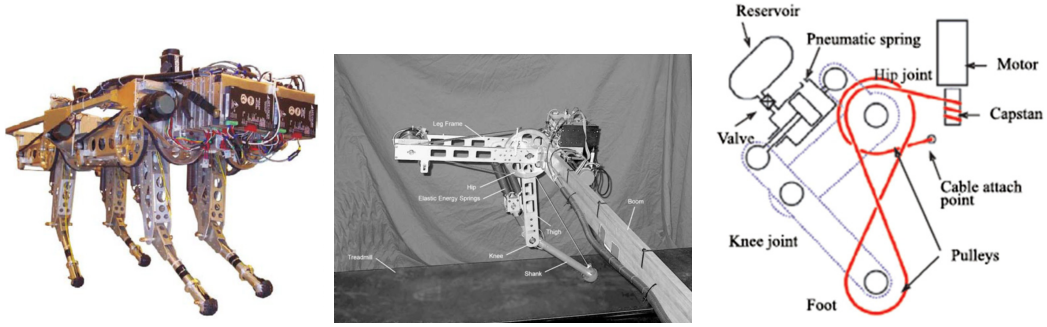

(a) (b) (c)

Figure 1.9: (a) The "KOLT" quadruped robot, (b) its electro-pneumatic leg and (c) the schematic of its thrusting system [10].

For the electro-pneumatic leg, the hip motion and knee motion are set to be decoupled with the help of a cable and pulleys, as shown in Figure 1.9c. A pneumatic spring is assembled in the thigh part to store elastic energy. The knee joint determines the leg stiffness, which is 15.9 kN/m with the leg fully extended. To connect the pneumatic spring and air cylinder, a check valve is used to retain the pressurized air

in the pneumatic cylinder.

For the compliant leg configuration, except for compressed air and steel coil springs, compliant mechanisms are also a potential option for the robotic leg design. Thanks to the development in manufacturing technologies and new materials, novel leg structures, in which every portion of each leg is elastic, have been designed. This configuration is widely applied in a variety of robots, such as "Bow Leg Hopper" [37] and "RHex" [38]. Using compliant material in the compliant legs is also an option to obtain leg compliance. Specifically, the "MABEL" robot incorporates the fiberglass into the transmission system [39]. Several robots apply flexure joints, such as "DASH" [40] and "HAMR3" [41]. The Sprawl robots incorporate flexural elements in hip joints to execute the rotation in both stroke and pitch directions [42].

1.3 Some Distinctive Mechanisms

Generally, there are three actuated DOFs in each leg for the quadruped robot. The foot-end is designed as a ball to minimize ground contact area. Since most of terrains provide few available footholds, the small contact area can provide better balance in the quadrupedal locomotion. However, in the robotic history, some distinctive structures have been developed to accomplish tasks in specific terrains.

1.3.1 Robots with One DOF for Each Leg

Usually, for a quadruped robot, each robotic leg has three actuated DOFs. There are two actuated DOFs in the hip to swing the thigh link in the frontal plane and lateral plane. An active rotational joint is assembled in the knee to swing the limb link in the lateral plane. The roll movement in the hip helps the robot not only to realize walking on an inclined slope in an upright stance but also to take turns during locomotion [13]. However, a quadruped robot has been developed by McGill University, whose leg has one actuated DOF. This mechanism can minimize the energy consumption and simplify the control strategy.

This special mechanism is developed by McGill University, which has been incorporated in two generations of four-legged robots "Scout I" (see Figure 1.10a) and "Scout II" (see Figure 1.10b). The "Scout" series are designed to perform the bounding gait[11]. In the locomotion, the robot never entirely left the ground. Each leg has only one actuated DOF, which is powered by an actuator in the hip [24]. Although

having a relatively simple mechanical design, the robot in the series can successfully achieve dynamic stability. "Scout II" is a self-propelled running robot, which has only one actuator for each hip as well [12]. Besides the hip actuator, a compliant prismatic joint is also incorporated in the leg. The controller can determine the locomotion of the robot by adjusting angular positions and torques of the front and hind legs [43]. The simplification for the leg structure can minimize the energy consumption and enhance mechanical reliability. With simple stiff legs, these quadruped robots can realize walking and stair climbing in bounding.

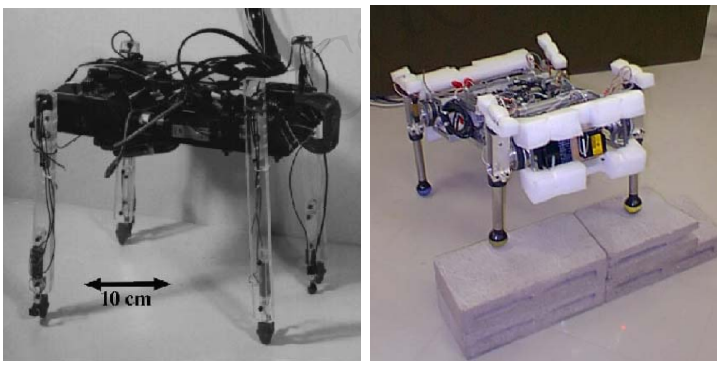

(a) (b)

Figure 1.10: Illustration of "Scout" series: (a) "Scout I" [11] and (b) "Scout II" [12].

Experimental results illustrate that "Scout II" can run up to 1.5 m/s in bounding. This robot is highly dominated by the passive dynamics to realize a high efficient energy transformation. Overall, "Scout" series set an example of using a relatively simple control strategy and a simple mechanical structure. However, the mechanical structure cannot actuate a compliant leg with a relatively long length. This disadvantage may restrict the available footholds on rough terrain.

1.3.2 Robots with Flexor Reflex

Normally, a small contact area at toes is widely used to increase the adaptability on irregular terrain, such as "LittleDog" from Boston Dynamics Inc. and "SQ3U" from Lynxmotion Inc. However, along with the development of the robot mechanism, novel structures have been designed for navigating and traversing rough terrain.

As a self-contained quadruped robot, "Tekken II" has been developed to incorporate novel mechanisms, which can be actuated on stumbling [13]. Similar to the configuration of "Tekken I", "Tekken II" is approximately 25% larger than the previ-

ous generation in both size and weight. As illustrated in Figure 1.11a, there are four joints on each leg of "Tekken II". DC motors (23 W) are used to actuate the hip joint around the pitch axis, while the motion around the yaw axis is activated by motors (8 W). A spring-lock mechanism is incorporated in the ankle joint. By controlling hip yaw joints, the locomotion direction can be adjusted. Rate gyros and inclinometers are applied to measure the pitch and roll angles of the body part.

The flexor reflex is designed to tackle the collision avoidance with obstacles. During the flexion phase of the step cycle, a stimulus on the paw dorsum produces an enhanced flexion in order to avoid obstacles. Inspired by a spinal cat, an ankle joint with a spring and a lock are designed in "Tekken I". This mechanism can realize obstacle avoidance by adjusting the posture of the foot-end during the first half of a swing phase. The sequence of flexor reflex is illustrated in Figure 1.11b [13]. In the first step (also called the flexor neuron active phase), the knee joint is flexed after the robot detects the stumbling. Then, the flexor reflex is lifted in the second step. After the leg escapes the stumbling condition, the ankle joint will move back to the initial situation. The flexor reflex can be triggered by enlarging the desired angle in a certain range. The knee joint angle can be measured at the moment of the flexor neuron active phase. Under the effect of the rubber elasticity, the ankle joint can return back to the initial angle, when the leg gets rid of the influence from obstacles. However, since lots of small bumps and pebbles present considerable friction on rough terrain, the passive ankle mechanism do not perform well in the outdoor environment.

Furthermore, "Tekken II" also applies other excellent structures to improve the locomotion performance, such as low leg inertia moment and powerful actuators. In addition, a small gear reduction ratio is applied to reinforce the compliance of joints.

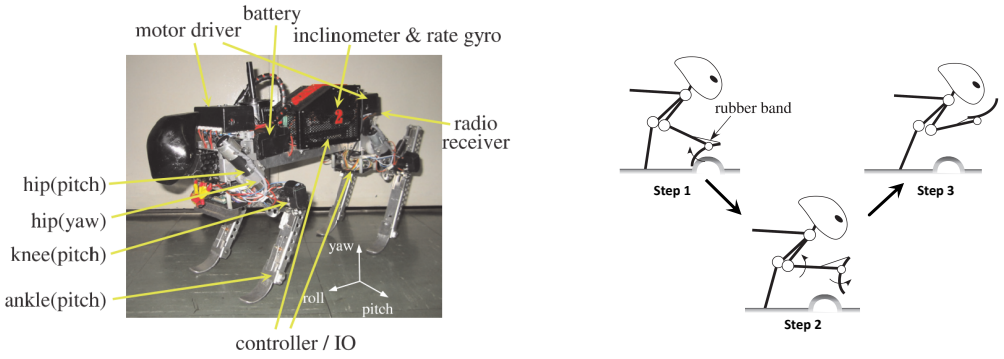

(a) (b)

Figure 1.11: (a)"Tekken II" and (b) flexor reflex activated on stumbling [13].

Table 1.1: Performance of representative quadruped robots developed in history.

Name	**Year**	**Mass** [kg]	$\frac{\textbf{Payload}}{\textbf{Weight}}$	**Gait**	$\mathbf{V_{max}}$ [m/s]	**DOF** (per leg)
"KUMO-I" [44]	1976	14	—	static	0.1	3
"PV-II" [45]	1979	10	—	static	0.1	3
"TITAN VI" [46]	1993	195	0.06	static	0.2	4
"JROB 1" [47]	1994	31.5	—	static	0.2	3
"Scout II" [12]	1998	2.3	0.02	dynamic	1.5	1
"RHex" [38]	1999	7	—	dynamic	0.4	1
"Tekken" [13]	2003	4.3	0.2	dynamic	0.9	4
"BigDog" [34]	2008	75	1.41	dynamic	3.1	3
"LittleDog" [31]	2011	2.8	—	static	0.1	3
"Cheetah II" [48]	2014	33	—	dynamic	6.4	3
"ERS-7" [49]	2017	1.5	—	static	0.3	3

1.4 Some Comments

Although quadruped robots have some distinct advantages comparing to other mobile robots, they have not been widely used in practical engineering field due to some limitations. For the traditional walking mechanism, such as four telescoping massless legs, the desired trajectory of the foot-end is limited by the set of singular configurations. Hence, quadruped robots have to adjust the step length to deal with obstacle avoidance with path planning. Besides, a comprehensive controller is implemented to manipulate four legs for rough terrain locomotion.

In addition, the payload is restricted by the strength of each joints. To minimize energy consumption, the quadruped robot should be designed in the lightweight construction. The injuries in the joints should also be avoided which might be caused by excessive musculoskeletal forces at collision.

Furthermore, noise from quadruped robots becomes one crucial problem, such as "LS3" from Boston Dynamics Inc. This limitation of the robot itself prevents the potential possibility of the battlefield, since a loud robot may give away their position. After all, it is relatively difficult to find a reasonable compromise in both decent payload and high-speed locomotion with low noise.

Quadruped robots can only perform tasks in some specific occasions to achieve limited goals. Moreover, the mechanical structure of the quadruped robot is also

determined by the working condition. Some exposed components will be corroded inevitably in hostile environments. For example, equipped with a pressure sensor and a signal processing system, the foot-end compromises the shape memory alloy, which may be damaged by friction and corrosion. Table 1.1 lists some quadruped robots developed in the last half century with main characteristics.

1.5 Thesis Organization

The thesis is organized as follows. Chapter 1 starts with reviewing the fundamentals and development of quadruped robots. The motivation of quadruped robots is highlighted in this chapter. The feature and performance of several typical quadruped robots are presented and compared.

The mechanical structure of the designed quadruped robot is described in Chapter 2, such as the body part, hip joint, thigh part, knee joint and limb part. Key components are also introduced, such as bevel gears, motors, potentiometers, ball bearings and timing belts. In addition, since the deformed shape may lead to structural failures, thereby influencing the quadrupedal locomotion. The finite element analysis (FEA) is performed when designing some structural components in reasonable structures. The design processes of the shoulder part and brass rod are described as examples.

Chapter 3 illustrates the modeling for a robotic leg and animated simulation of the designed quadruped robot in MATLAB. Kinematic models and Euler-Lagrange equations are formulated for the robotic leg. An animated simulation of the quadrupedal locomotion is emulated with the creeping gait. The desired trajectory of the foot-end is also determined to avoid the set of singular configurations. Euler-Lagrange equations are calculated in the MATLAB/SimMechanics model to compute the actual joint angles. PD control is implemented to track the desired trajectory. The evaluation of simulation results is also presented in Chapter 3.

Chapter 4 summarizes the work in this thesis. The future work is also presented in this part.

Chapter 2

Mechanical Design of a Quadruped Robot

This chapter focuses on the mechanical design of the designed quadruped robot which is composed of a body part and four compliant legs. To simplify the mechanical structure of the designed quadruped robot, the mass distribution is symmetrical about the frontal and lateral planes. The mechanical structure is built in a computer-aided design (CAD) model (see Figure 2.1). Particularly, the leg mechanism includes a hip joint, a thigh part, a knee joint and a limb part with a telescoping joint. In the sequel, we will introduce the mechanical structure of each part.

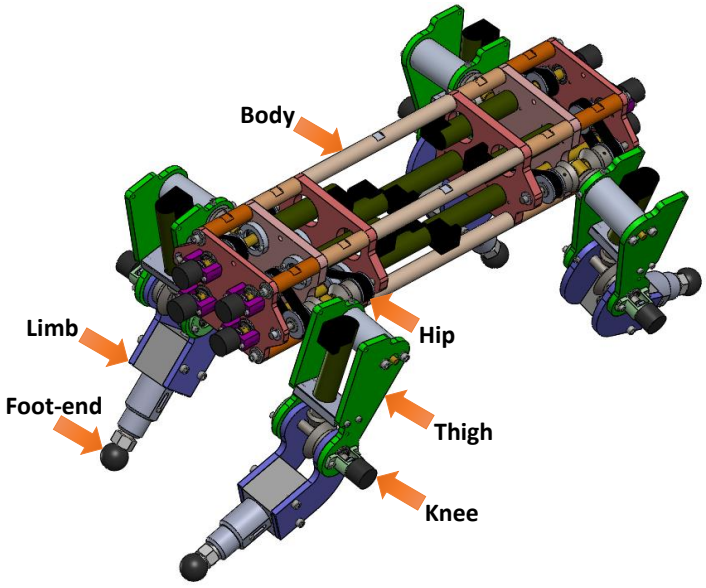

Figure 2.1: The CAD model of a quadruped robot.

2.1 Design Principles

Inspired by the "LittleDog" design in [31] from Boston Dynamics, Inc., a quadruped robot is designed for research purposes, such as legged locomotion and autonomous navigation. The system energy flow of a typical quadruped robot is illustrated in Figure 2.2a. The Joule heating loss mainly occurs at the rotating motor side and the printed circuit board (PCB). Besides, some mechanical energy is consumed due to the mechanical transmission friction and interaction friction. To minimize the energy consumption, some principles are illustrated in Figure 2.2b, including high torque density motors, reverse current braking, low impedance transmission, low friction in rotational joints, low inertia legs and internal energetic conversion [50]. To realize these design principles for energy efficiency improvement, several mechanical structures and appropriate components have been designed, as illustrated in Figure 2.2c. These principles are implemented in the mechanical design of the quadruped robot.

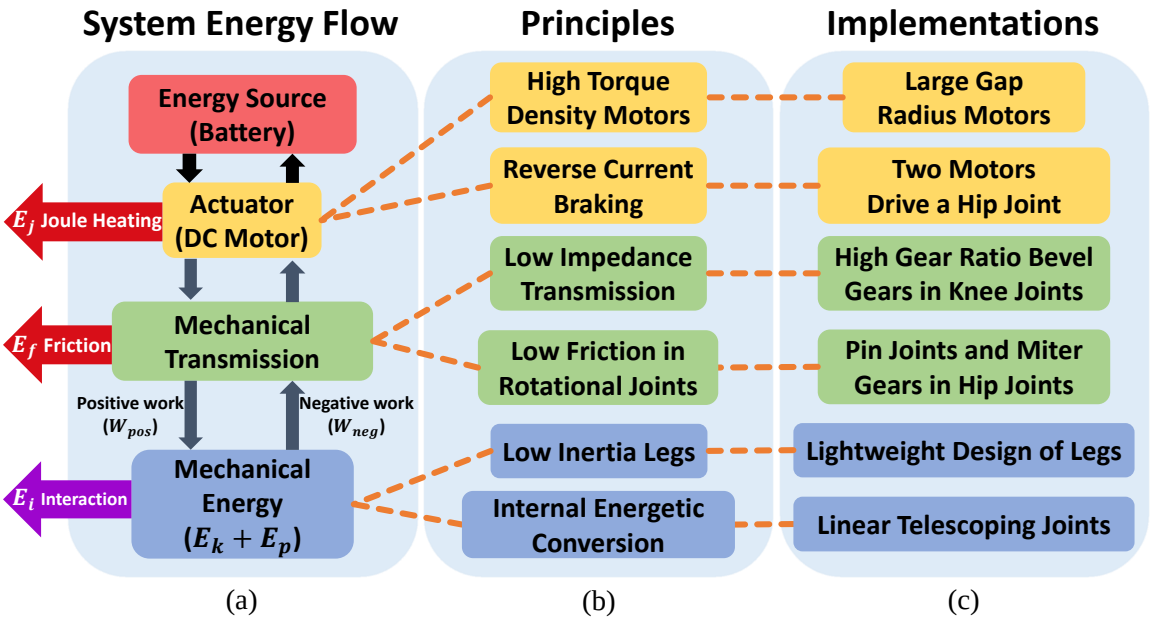

Figure 2.2: (a) Energy flow diagram of the quadruped robot. (b) Design principles to improve energy efficiency. (c) Strategies to implement design principles.

The designed quadruped robot comprises the body part and four compliant legs. The mass of the body is 4 kg, and the mass of each leg is 1 kg. The whole robot is actuated by twelve motors to perform passive dynamic walking. The rotation angle of each motor is measured by a potentiometer.

Table 2.1: Design parameters for the quadruped robot.

Parameters	**Value**
Body length	0.521 m
Body width	0.146 m
Body thickness	0.095 m
Leg length	0.152 m
Ground clearance	0.254 m
Body mass	4 kg
Individual leg mass	1 kg
Total mass	8 kg
Leg spring compliance	5250 N/m
DC servo motor	Swiss Maxon DC motor 41.022.022
Potentiometer	SAKAE 22HP-10 20 KΩ

2.2 The Main Body Structure

To reduce the mass of the platform, the components with small sizes and mass are selected to realize a lightweight design. The designed quadruped robot is mainly constructed by aluminum alloys 6061, which is a high strength material with a great range of mechanical properties. The key components are assembled in the main body part as many as possible, as shown in Figure 2.3. In this way, the leg weight is reduced as much as possible to improve the leg agility. Besides, the lightweight design of leg links can ensure low rotational inertia and reduce the payload for actuators. Hence, the body part is designed to comprise eight motors, eight potentiometers, sixteen bearings and eight timing belts. These components are symmetrically distributed in the body part. Particularly, a timing belt, which transfers the power from the motor side to the hip joint side, is chosen to connect two synchronizing pulleys.

2.2.1 Aluminum Plates

The body part is designed as a symmetrical structure. To assemble key components in the body part, three types of aluminum plates are machined, as shown in Figure 2.4. Two pieces of each type are placed in the front and back of the body part, respectively. Two pieces of the aluminum plate A, as shown in Figure 2.4a, are placed at two ends

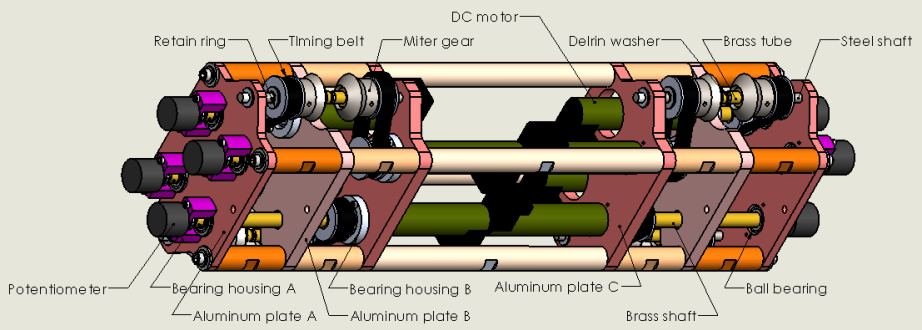

Figure 2.3: The CAD model of the body part.

of the body part. As shown in Figure 2.4b and Figure 2.4c, the other two types of aluminum plates are assembled in the body part, respectively. These six plates are used to fix two types of brass shafts via sixteen ball bearings.

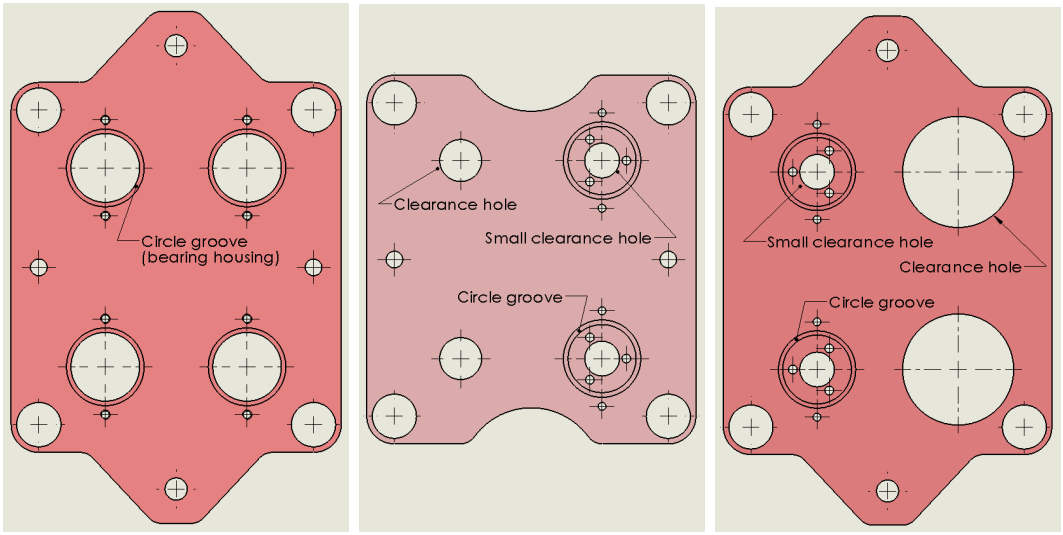

(a) (b) (c)

Figure 2.4: Illustration of three types of aluminum plates in the body part: (a) the aluminum plate A which is assembled to fix the potentiometer at both ends of the body part, (b) the aluminum plate B which is machined to clamp the motor and (c) the aluminum plate C which is mounted in the middle of the body part to clamp the motor.

Four circle grooves are machined on the surface of the aluminum plate A as bearing housings to clamp four ball bearings. Two clearance holes and two circle grooves (play a role as bearing housing) are manufactured in each piece of the other two types of plates. Particularly, the clearance holes in Figure 2.4b and Figure 2.4c are machined for brass shafts and servo motors, respectively. The brass shaft is used to connect

the motor, pulley, ball bearing and potentiometer to transmit the actuating torque. Hence, the potentiometer can measure the angular position of the motor shaft. The pulley can transmit the actuating torque to the hip joint. Two types of bearing housings are designed to be mounted on the body part, as shown in Figure 2.5. The bearing housing A in Figure 2.5a is assembled in the middle of the body part to clamp the ball bearing. The bearing housing B in Figure 2.5b is placed on aluminum plates, which are illustrated in Figure 2.4b and Figure 2.4c. This bearing housing not only can help the ball bearing to clamp the brass shaft, but also can fix the housing of the potentiometer.

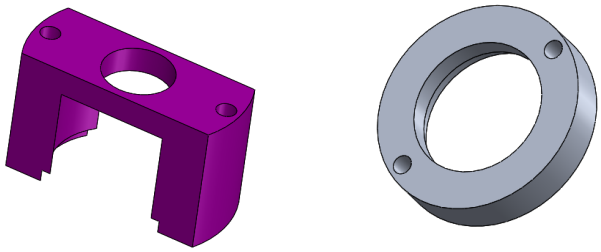

(a) (b)

Figure 2.5: Illustration of two types of bearing housings in the body part: (a) the bearing housing A to fix the potentiometer at both ends and (b) the bearing housing B to clamp the ball bearing in the middle portion.

2.2.2 Motor Selection

Twelve motors are assembled in the quadruped robot to actuate four hip joints and four knee joints. Eight of them are assembled in the body part, and one motor is assembled in each thigh part of legs. The motor is appropriately selected to provide the sufficient torque to the joint without loss of motion, meaning that no skipping or slipping happens in the quadrupedal locomotion. To provide a sufficient driving torque to help bevel gears to perform effective rotations, the low-speed/high-torque motor is selected as the actuator.

The Swiss Maxon DC motor with a dual encoder is selected as the actuator in the designed robot. The rated speed of the motor is 46 revolutions per minute (RPM), and the rated power is around 5 W. With the help of bevel gearboxes, actuating forces are redirected in both hip joints and knee joints. Generally, to assemble a motor in

the robot, three screws are used to fix the motor at the aluminum plate B and C. In the aluminum plate B and C, small clearance holes are machined to clamp motors. To actuate the hip joint, motors are horizontally fixed on the aluminum plate B and C, which are shown in Figure 2.4b and Figure 2.4c. Through brass shafts, motors in the body part are connected to potentiometers. Meanwhile, the torque is transformed from the motor side to the drive gear by the timing belt.

(a) (b)

Figure 2.6: Illustrations of the motor and its connection: (a) the Swiss Maxon DC motor and (b) the CAD model to illustrate the connection of the motor, aluminum plate and bevel pinion.

2.2.3 Timing Belts

Eight timing belts are used to transfer the actuating torque from the motor shaft to the steel shoulder shaft. To improve the measurement accuracy, aluminum alloy synchronous pulleys, with 24 teeth and a diameter of 10 mm, are chosen as the timing belt. Hence, these two pulleys can rotate at the same speed, and the torque generated from the motor side can be transmitted to the joint side. By applying this design, the load can be successfully sustained on the teeth of gears with an acceptable deflection. To improve the torque transmission efficiency, the distance between two pulleys is chosen such that the belt is assembled with an appropriate tension, otherwise, the excessive tension will add extra stress on the belt. A proper belt tension can avoid slipping in a high load or bearing an extra load. In tests, we measure the load in different center distances between two synchronous pulleys. Based on measurement results, the appropriate distance is chosen as 44.5 mm to ensure proper belt tension.

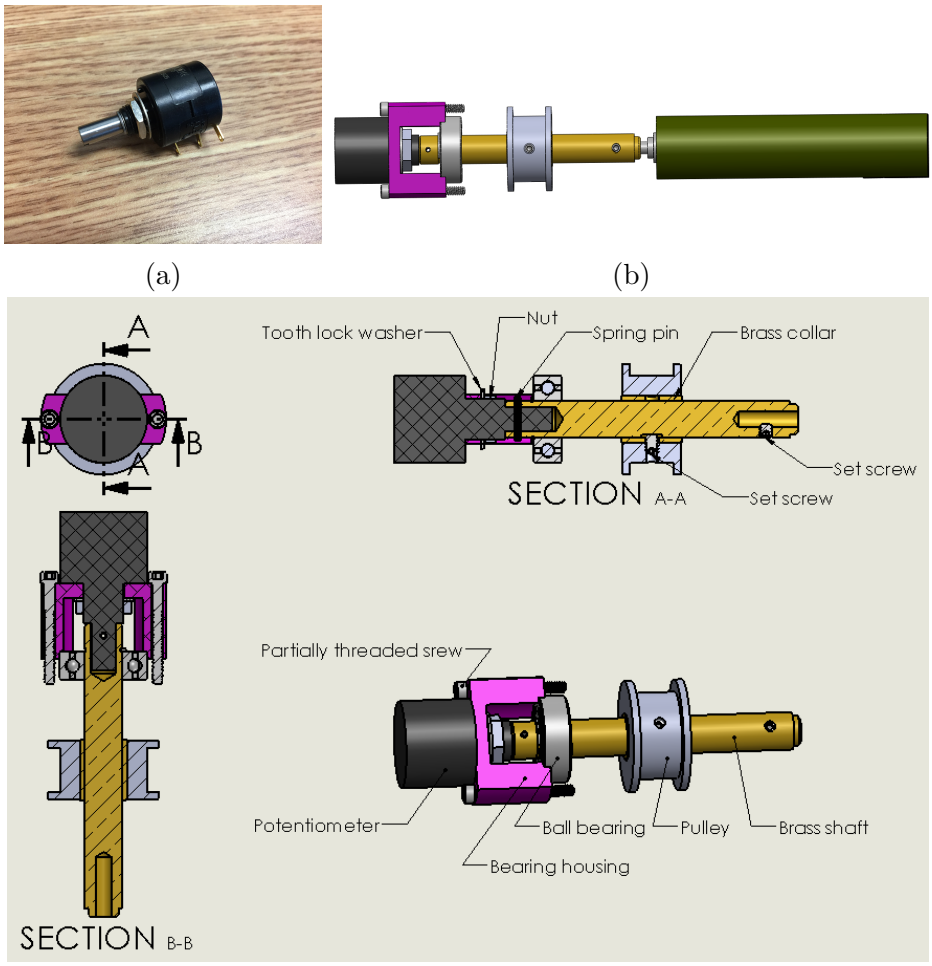

Figure 2.7: Illustrations of the potentiometer and its connection: (a) the potentiometer–SAKAE 22HP-10, (b) the CAD model of the connection among the motor, two bearings, two types of bearing housings and the potentiometer and (c) section views of the CAD model without the motor.

2.2.4 Potentiometers

SAKAE 22HP-10 potentiometers, pictured in Figure 2.7a, are chosen because of their precise $\pm 0.25\%$ linearity to the measurements of the angular positions of the hip and knee joints. The potentiometer is a three-terminal resistor whose rated power is 2 W and the resistance is 20 KΩ. To measure the angular position of the hip joint, a brass shaft is used to connect the shafts of the potentiometer to motor by a spring pin and a set screw, respectively. By using a nut and a tooth lock washer, the housing of the potentiometer is clamped to the bearing housing and fixed to the aluminum plate in

the body part. The angular position can be measured by the angle difference between the shaft and the housing of the potentiometer.

Figure 2.7b illustrates the connection among the motor, pulley, and potentiometer in the body part. A brass shaft is used to transmit the actuating torque from the motor side to the joint side. To prevent bending or twisting in the brass shaft, the shaft length is designed as short as possible while the position of the motor is appropriately selected. Two bearings are used to fix the brass shaft to two aluminum plates. The motor is placed at one end of the brass shaft, while the potentiometer is mounted on the other end. The similar structure is applied to measure the angular position of the knee joint.

2.2.5 Gears

The bevel gearbox plays a central role to transmit the torque from the motor side to the joint side and change the operating angle. Bevel gears in the designed quadruped robot are mounted on shafts, which are capable of supporting high forces and are 90° apart. To reduce the risk of skipping in the hip joint and knee joint, large gears with deep teeth are selected. In addition, couplings are not implemented in the body and compliant legs, which reduces the possibility of slipping.

For the hip joint, to execute the rotation of the thigh part, miter gears are mounted on a brass rod and two brass tubes. Unlike the mechanical structure of the hip joint, the knee joint is actuated through a bevel gear pair with a 5:1 ratio. Either type of joints transmits the rotational motion at a 90° angle. To actuate the joint effectively, bevel gears should be precisely mounted on the input link and the output link. In addition, to avoid concentrating the load at the end of the tooth, bevel gears should be assembled with minor adjustments. This assembly allows the displacement of bevel gears, which are caused by deflection under operating loads. The incorrect installation may damage the joint.

2.3 The Leg Structure

Four compliant legs are designed to connect the body part. Each leg consists of a hip joint, a thigh part, a knee joint and a limb part. To design artificial quadruped legs, desired characteristics, such as speed, endurance, agility and strength, are incorporated into mechanical design. To realize these characteristics, main considerations

are summarized in Table 2.2 and are enumerated as follows:

- The effective leg length will influence the speed of movement and the agility of the leg. The stride length can be increased by extending the leg length. Hence, the mobile speed of the quadruped robot can be improved. In addition, extending the leg length can reduce the energy cost of transport, thereby improving the endurance.
- Mass distribution affects the speed of movement by influencing the stride frequency. In this way, the posture of the robotic leg would be easily controlled, when key components are assembled in the body part as many as possible.
- Leg kinematics determines the endurance. The hip joint can rotate in the frontal plane and lateral plane. The knee joint rotates in the frontal plane. The bevel gear pairs with high gear ratio is supposed to be used in the joints to reinforce the endurance. As a prismatic joint, the compressed spring can be assembled in the limb link to adjust the leg stiffness and to absorb the impact at collision.
- Elastic energy storage in tendons improves agility. By applying internal energetic conversion, the compressed spring can improve the endurance. The tendon stiffness influences the duration of the stance phase.
- Muscle power is determined by the actuating torque, which is provided by the DC motor. Hence, the speed and strength of the compliant leg are influenced by the rated power of the motors.

Table 2.2: Key elements and their influence on desired characteristics.

	Speed	**Endurance**	**Agility**	**Strength**
Effective length	✓	✓		
Mass distribution	✓		✓	
Kinematics		✓		✓
Elasticity	✓	✓	✓	
Muscle power	✓			✓

In the process of the leg design, above elements are taken into consideration. Table 2.2 demonstrates the relationships between desired characteristics and technological instantiations.

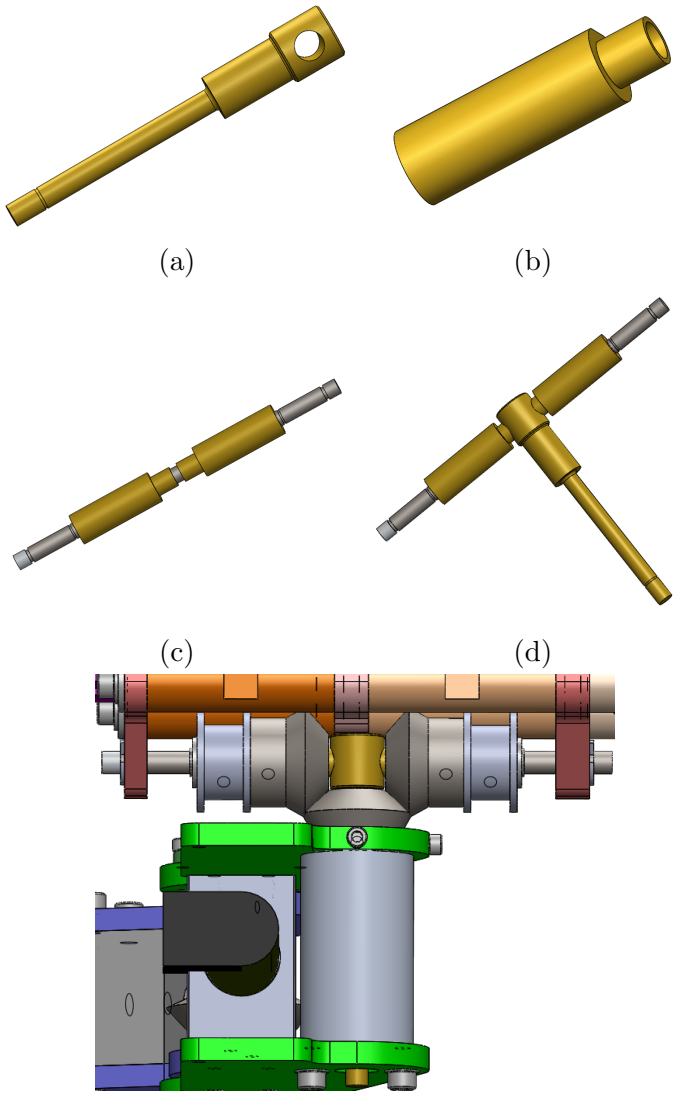

Figure 2.8: Illustrations of the structure in the hip joint: (a) the brass rod, (b) brass tube, (c) shoulder part, (d) pin joint and (e) key parts of the hip joint.

2.3.1 Hip Joint Design

Hip joints are supposed to be strong enough to support the body weight including some attached peripherals in the stance phase. Besides, the hip joint should be able to sustain the leg weight in the swing phase. The hip joint comprises the shoulder part, the brass rod, three bevel gears and two pulleys. As shown in Figure 2.8c, the shoulder part is composed of a steel shaft and two brass tubes. Figure 2.8d illustrates the connection of the pin joint, which consists of the shoulder part and the brass rod.

To provide the support force in the hip joint, three bevel gears are mounted in the pin joint. The steel shoulder shaft and brass rod are perpendicularly assembled. For each hip joint, two bevel gears are mounted on two brass tubes which are placed in the steel shaft as drive gears. The third one is mounted on the brass rod which is placed in the thigh part as the drive gear. For each hip joint, two miter gears are mounted on two brass tubes, and are driven by two groups of timing belts separately. Since two bevel gears are actuated by two motors, they do not need to synchronize with each other. When rotating directions of the two gears are the opposite, the thigh part swings forward or backward. When rotating directions of the two gears are the same, the thigh part is actuated to move in the frontal plane. By controlling the angle difference between gears, the direction of the quadrupedal locomotion can be adjusted. Mounted on two brass tubes, two drive gears are able to rotate in opposite directions. These two tubes are assembled on the shoulder steel shaft and are separated by two delrin washers. The steel shaft connects two aluminum plates of the body part. Two delrin washers can avoid the friction loss between two brass tubes. With the help of the lubricant, two brass tubes can rotate around the steel shaft flexibly.

On the leg side, the hip joint of the quadruped robot is designed in a frontal and vertical sliding mechanism. The pin joint (see Figure 2.8e) prevents the leg from rotating in the horizontal plane. Additionally, when the drive gear rotates around the brass rod, the angular offset is transferred to the hip joint to actuate the thigh part.

Furthermore, the position of the drive gear is determined by the length of the brass rod. The hip joint can transmit the actuating torque efficiently through the miter gearbox. Correct assembly of three miter gears can avoid skipping in the mechanical transmission.

2.3.2 Thigh Part Design

For each compliant leg, a motor is mounted between thigh rails to actuate the knee joint. Although the traditional serial link robot increases the inertia of the distal links, the benefit arises in the simplification of the control strategy.

To reduce the weight of the whole robot, one potential solution is to shorten the leg length. However, thigh rails should be designed to cover the motor and to protect components from unexpected forces, as shown in Figure 2.9a. In addition, designed

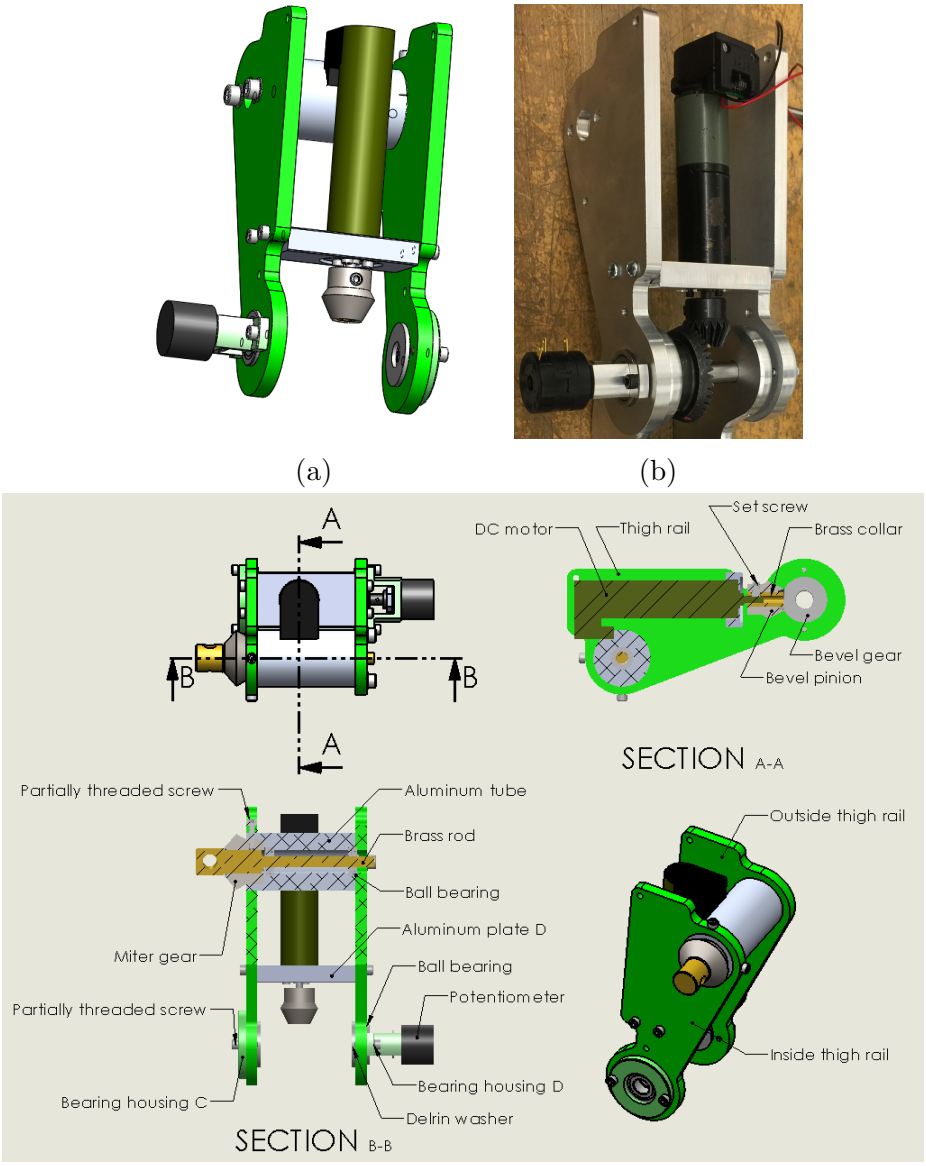

Figure 2.9: Illustrations of the thigh part: (a) the CAD model of the thigh part with the brass rod, (b) the assembly of the thigh part and (c) Section views of the CAD model of the thigh part with the brass rod.

with sufficient lengths, leg links can help the robot to step onto or over obstacles. After taking above factors into consideration, the lengths of the thigh link and limb link are both selected around 0.15 m. The step height can reach up to approximately 0.1 m.

As shown in Figure 2.9c, two partially threaded cap screws are applied at the side

surface to fix the inside thigh rail, aluminum tube and driven gear. On the one hand, the inside thigh rail and aluminum tube are machined with two clearance holes at their side surfaces. On the other hand, two threaded holes are machined in the side surface of the driven gear. For each hole, a partially threaded cap screw is used to fix the thigh rail, aluminum tube and driven gear successively through these holes at the side surface. The aluminum tube connects the brass rod through two ball bearings. Besides, circle grooves are machined in thigh rails and aluminum tubes as bearing housings, which are used to clamp ball bearings to hold the pin joint, as shown in Figure 2.10b. Two partially threaded cap screws are applied to fix the outside thigh rail and aluminum tube through the clearance hole and threaded hole.

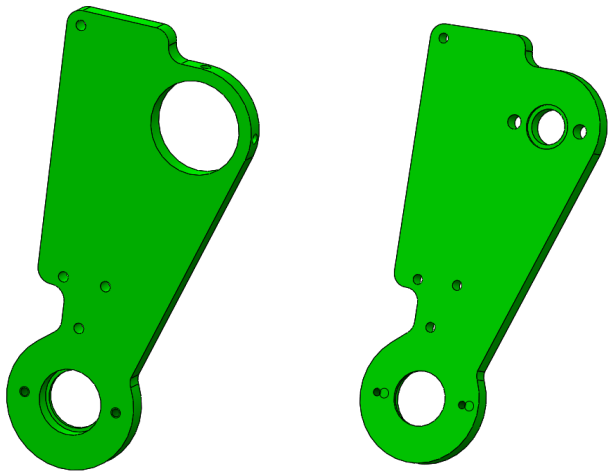

(a) (b)

Figure 2.10: Illustrations of the CAD model of thigh rails: (a) the inside thigh rail and (b) outside thigh rail.

As illustrated in Figure 2.10, the inside and outside thigh rail have the similar outline. However, the upper portions of these thigh rails are different. Figure 2.10a shows that two clearance holes are machined in the side surface. A relatively large hole is designed for the aluminum tube to be assembled. As shown in Figure 2.10b, a cycle groove is machined in the outside thigh rail as a bearing housing. Two clearance holes are manufactured for two cap screws to fix the aluminum tube to the outside thigh rail. For each thigh part, a motor is placed vertically between thigh rails to actuate the knee joint. The actuating force is redirected by a bevel gearbox. An aluminum plate is placed horizontally between thigh rails to clamp the motor. Moreover, this aluminum plate is fixed by four standard rounded head screws to provide a channel

bracing for thigh rails to avoid collapsing. A bevel pinion is mounted on the motor shaft through a collar.

2.3.3 Knee Joint Design

The knee joint is actuated by a bevel gear pair with a 5:1 ratio. By applying the bevel gearbox, the actuating force is redirected to drive the limb part. The bevel pinion is vertically placed between thigh rails. A set screw is applied to fix the bevel pinion to the motor shaft. The thread size of the set screw is M3, and its length is 3 mm. The driven gear is mounted on the steel shaft by a steel pin. Two alloy steel flat-tip set screws are used to fix the driven gear to the outside limb rail. The steel shaft is fixed to the inside limb rail by a partially threaded screw on the side surface. The steel shaft is applied to connect the thigh rails through two ball bearings. Overall, the motor drives a bevel pinion to actuate the limb part via a large couple gear. Meanwhile, the pair of straight-tooth bevel gears, being mounted on perpendicular shafts, is used to transmit torques from the motor side to the joint side.

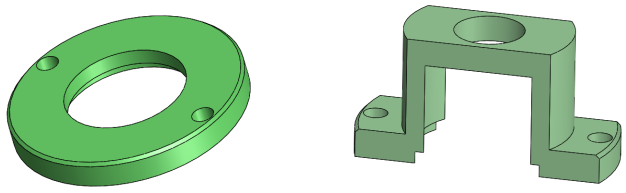

(a) (b)

Figure 2.11: Illustrations of two types of bearing housings in the knee joint: (a) the bearing housing C to fix the potentiometer at the outside thigh rail and (b) the bearing housing D to clamp the ball bearing at the inside thigh rail.

Potentiometers are assembled to measure the angular position of knee joints. Ball bearings are mounted on thigh rails to fix rotating shafts and are clamped by bearing housings. The stress pattern is press-fit among the brass rod, ball bearing and thigh rail. Two ball bearings are assembled to fix both ends of the brass rod. Each ball bearing is clamped by an aluminum plate and a bearing housing. Two types of bearing housings are used in the body part. As shown in Figure 2.12, the potentiometer is fixed on the brass shaft by a spring pin. The potentiometer can obtain the angular position of the knee joint by measuring the deviation between the thigh part and limb

part. On the one hand, the knee brass shaft and bevel gear rotate with the limb and the shaft of the potentiometer. On the other hand, the housing of the potentiometer rotates with the thigh part. Hence, the measured information can be transmitted to the controller in real time.

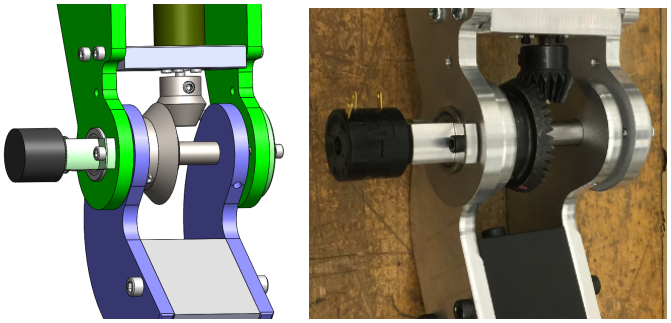

(a) (b)

Figure 2.12: Illustrations of the knee joint: (a) the CAD model to illustrate the knee joint and (b) the mechanical structure of the knee joint.

2.3.4 Limb Part Design

The compression spring is incorporated into the limb structure design. This mechanism can not only prevent the impact at collision, but also can change the limb length in the locomotion. To meet the required stiffness of the limb, a compression spring with the appropriate compressed rate should be carefully selected. Consequently, the linear telescoping joint is included in the limb part to adjust the leg length. Mutual transformations between the kinetic energy and potential energy are realized by utilizing the inherent compliance behavior of the telescoping joint. When the foot-end sustains an exterior force, the telescoping joint will be compressed. Then the compressed gas and mechanical spring provide a high force to the compliant leg. Meanwhile, the high pressure from the foot-end increases the stiffness of the limb part and reduces the duration of the stance phase.

As shown in Figure 2.13b, the delrin tube and rod are machined to be press fit. The mechanical spring not only absorbs energy from the external load such as the unexpected impact from the ground, but also reduces the energy cost during the continuous movement by applying internal energy conversion. By performing a relatively high-frequency hopping in a reasonable stride length, the compliant leg can realize the resonant bounding motion. In this way, the quadruped robot can

perform multi-modal locomotion, such as the trotting gait, pacing gait and bounding gait. This special mechanism reduces the energy consumption during continuous leg movements, and the passive prismatic joint can reduce the vibration of the body part effectively. Moreover, all parts should be machined within an appropriate tolerance in the machining process. Otherwise, machining errors may cause unsuccessfully installation, which may damage the mechanical structure.

2.4 Finite Element Analysis

Accurate physical models of the designed quadruped robot is drawn in the CAD software. Besides, the predefined information of the designed CAD quadruped model is illustrated in SolidWorks, such as masses and link lengths. Since the deformed shape may lead to structural failures, the finite element analysis (FEA) is performed when designing some structural components. After finding out the fragile portion of the whole robot, we can strengthen the designed mechanical structure by selecting proper materials and designing reasonable structures.

Generally, bending and twisting may happen in long brass shafts, when they sustain extensive payloads. For example, in the body part, a brass shaft is used to connect a motor to a potentiometer. This brass shaft also transfers the motor torque to actuate the hip joint through timing belts and gearboxes. In this process, the brass shaft suffers from the compressive stress and tensile stress, and the deformation of the shaft may be triggered. The deformed shape may lead to structural failures, thereby influencing the quadrupedal locomotion. By applying FEA to the CAD model, the extreme pressure-point can be found. Several actions are taken to strengthen the fragile position by adjusting the shape and material of structural components.

2.4.1 FEA for the Shoulder Part Design

The shoulder part is expected to sustain the leg weight in the swing phase and to support the body weight in the stance phase. FEA is applied in the process of the shoulder part design. In the shoulder part, two brass tubes are mounted on the steel shaft.

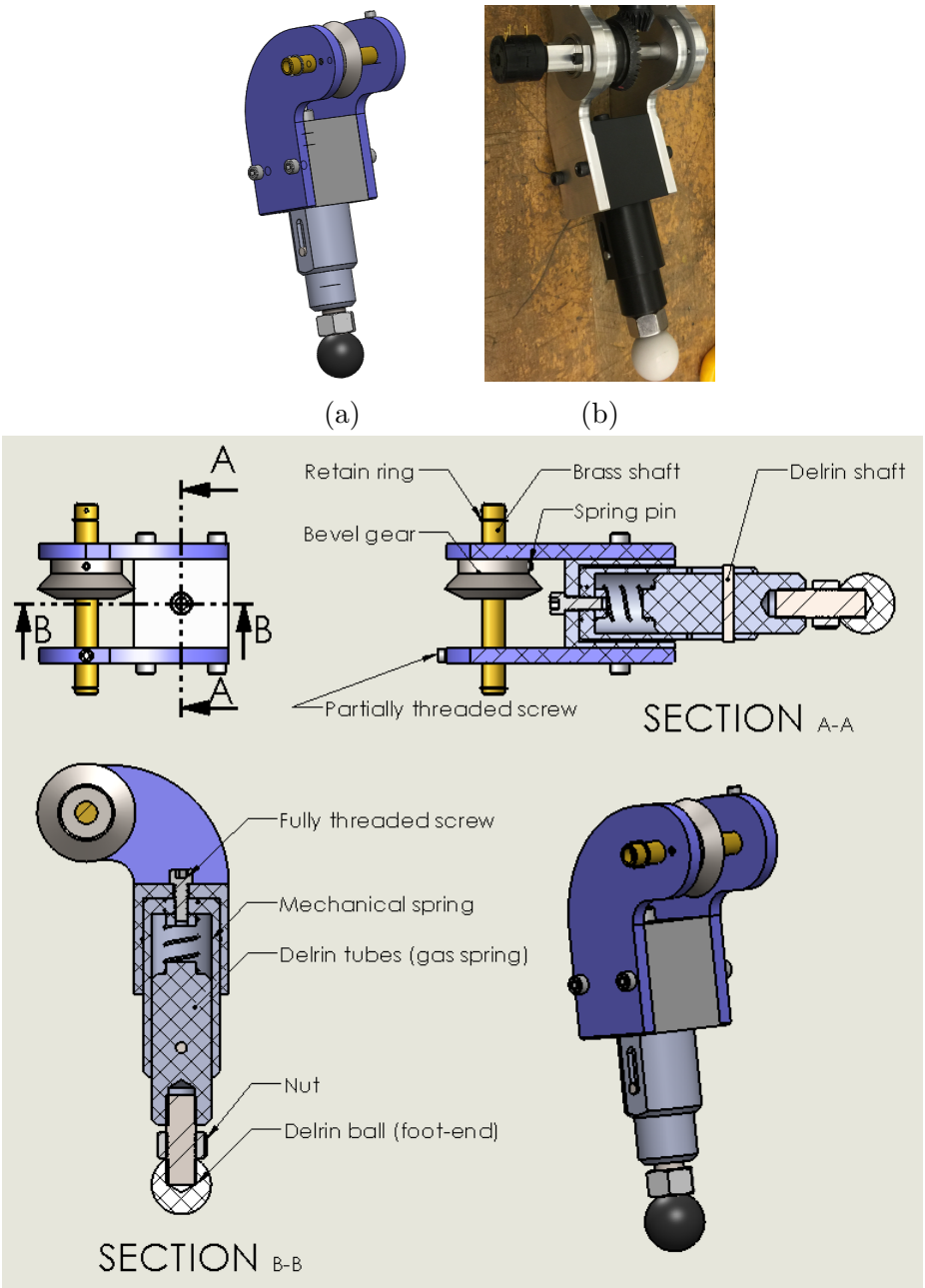

(a) (b)

(c)

Figure 2.13: Illustrations of the limb part: (a) the CAD model of the limb part, (b) the assembly of the limb part and (c) section views of the CAD model of the limb part.

Loads and Fixtures

In the FEA simulation, the shoulder part sustain the leg, whose mass is 1 kg. Hence, the load is set as 10 N and distributed in the small cylinder portions of two brass

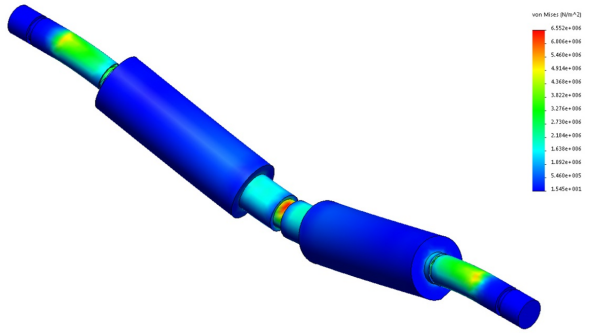

(a)

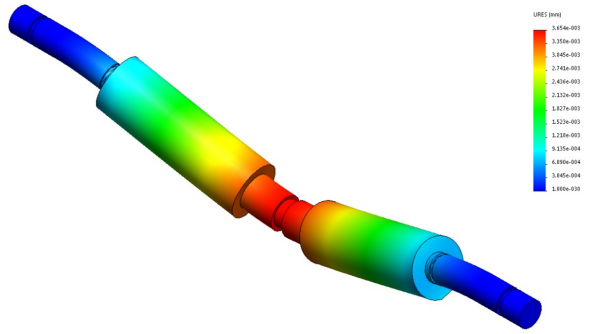

(b)

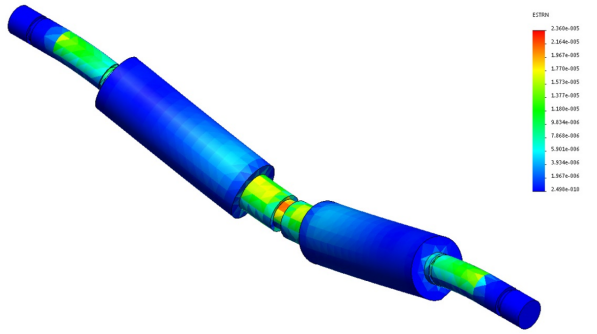

(c)

Figure 2.14: Illustrations of analysis results for the shoulder part: (a) von Mises stress, (b) resultant displacement and (c) equivalent strain.

tubes. As shown in Figure 2.8e, the steel shaft is fixed to the body part by two aluminum plates. The fixture type is set as fixed geometry. Based on the above information, the strain distribution is analyzed.

Results

Figures 2.14 illustrates the compressive and tensile strain distribution of the steel shoulder shaft with two brass tubes. As mentioned in Section 2.1, a steel shaft connects two aluminum plates and provides a support force for the compliant leg in the swing phase. Two brass tubes are mounted on the steel shaft. A gear and a pulley are mounted on each of brass tubes to actuate the hip joint. Hence, two miter gears are able to rotate against each other. Figures 2.14a shows the distribution of von Mises strain in steel shaft. The von Mises strain of the shoulder part is distributed along lines extending from two ends to the midpoint. The transverse compressive strain is mainly distributed in the middle position of the steel shoulder shaft and the area around grooves. As shown in Figure 2.14a, the minimum von Mises stress is approximately 15.45 N/m^2. The utmost pressure-point is the midpoint of the steel shaft, which sustains 6.55×10^6 N/m^2.

Figure 2.14b illustrates that the maximum displacement of the shoulder part is 3.65×10^{-3} mm. In Figure 2.14c, the equivalent strain of the steel shaft with two brass tubes presents a range from 2.50×10^{-10} to 2.36×10^{-5}. Overall, these analysis results show the stress condition of the shoulder part. The mechanical structure meets the expected stress distribution.

2.4.2 FEA for the Brass Rod Design

In the shoulder part, two brass tubes are mounted on the steel shaft. With the help of the lubricating oil, two tubes can rotate against each other. Two delrin rings are used to separate two tubes to prevent the frictional loss. The outside diameter of the delrin ring is smaller than the outside diameter of the brass tube. By adjusting the size of the delrin ring, the extra frictional loss can be avoided. The brass rod can provide the support force to the steel shaft, which is the utmost pressure-point in the shoulder part. In this way, the support force of the hip joint can be enforced to sustain the leg weight.

For the hip joint, the brass rod sustains the leg weight during the swing phase and bears the body weight during the stance phase. By applying the FEA, we optimize the shape of the brass rod. After several tests, the brass rod is determined as Figure 2.6a. The model information and study result of the brass rod is illustrated in sequence. The structure of the shoulder part is determined according to the data of the von Mises stress, resultant displacement and equivalent strain.

Loads and Fixtures

The brass rod sustains a reaction force 10 N through a driven gear and two ball bearings, as shown in Figure 2.9c. Particularly, the bevel gear is mounted on the middle cylinder of the brass rod. Two ball bearings are used to fix the small cylinder of the brass rod to the aluminum rod. Hence, the force is applied on three contact faces. For the fixture details, the clearance hole in the brass rod is set as the fixture, whose type is fixed geometry.

Results

Figure 2.15 shows the analysis results of the brass rod, such as the distribution of compressive and tensile stresses.

In Figure 2.15a, the von Mises stress of the brass rod ranges from 8.71 N/m^2 to 2.09×10^6 N/m^2. The data of von Mises stress illustrates that the utmost pressure position is the connection area between the small brass cylinder and middle brass cylinder. In addition, the yield strength of the brass is 2.39×10^8 N/m^2. Hence, the maximum pressure on the brass rod is smaller than the yield strength of the material. The brass rod can successfully sustain the leg weight.

Figure 2.15b shows the resultant displacement, when the load is applied in the brass rod. As expected, the connection portion between the small cylinder and middle cylinder sustains the maximum deflection. The maximum resultant displacement is approximately 9.44×10^{-3} mm.

Figure 2.15c shows the distribution of equivalent strain in the brass rod. The area between two cylinders of different diameters sustains the maximum equivalent strain, which is 1.50×10^{-5}. The plot indicates the minimum equivalent stain is 5.71×10^{-10}.

In summary, from the FEA of the shoulder shaft, the middle portion sustains extensive pressure. A brass rod is designed to provide a support force by wrapping this fragile position. Hence, the shoulder part and brass rod constitute a pin joint which is the key part of the hip joint to execute the leg movement. The brass rod can help the shoulder part to sustain the leg weight in the swing phase and to bear the body weight in the stance phase. In addition, to reduce the pressure of the fragile portion of the steel shaft, three miter gears are mounted in the hip joint to bear the load as well. In this way, three miter gears not only drive the thigh part accurately, but also to some extent bear the leg weight during the swing phase.

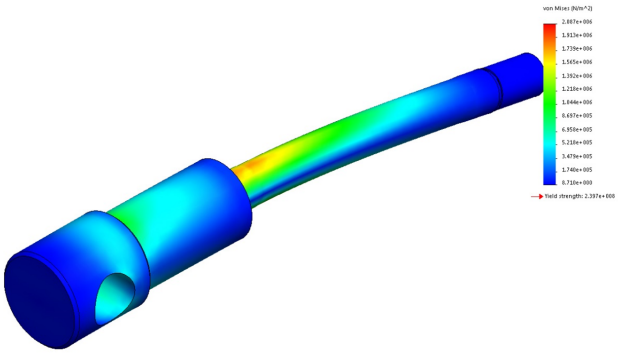

(a)

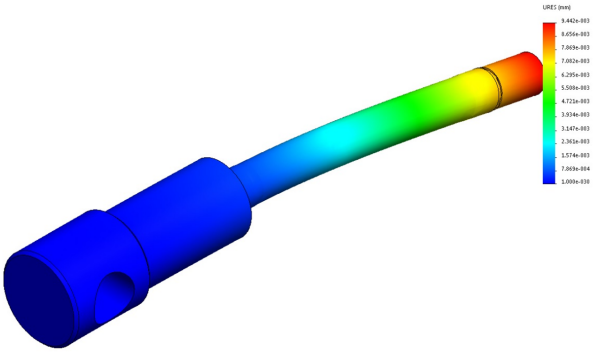

(b)

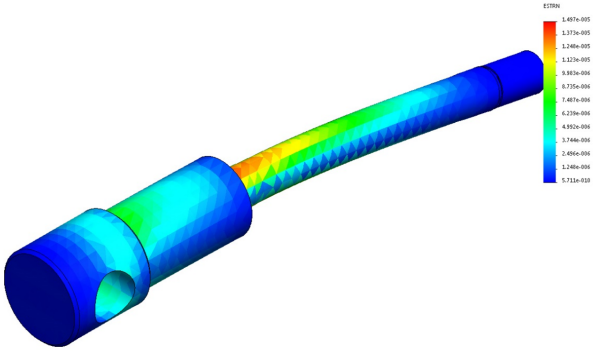

(c)

Figure 2.15: Illustration of study results of a brass rod: (a) von Mises stress, (b) resultant displacement and (c) equivalent strain.

2.5 Conclusions

In this chapter, the mechanical structure of the designed quadruped robot is illustrated, aiming to develop a legged robot. The designed symmetrical structure can realize the bi-direction locomotion and simplify the control problem to some extent.

The mechanical design consists of main body design, compliant leg design, joint design, and component selection. From the mechanical perspective, the inertia of the body and leg is reduced by adjusting the positions of components and by changing the shapes of thigh and limb rails. Besides, to increase the stiffness of the compliant leg, a linear telescoping joint is incorporated into the limb part. The passive prismatic joint is included in the leg structure to absorb the impact force at collision and to prevent unforeseen perturbations in a passive way. With the designed mechanical structure, the quadruped robot can perform various types of behaviour gaits, such as trotting, pacing and bounding.

The mechanical structure of the quadruped robot is analyzed and verified by the FEA simulations. The shoulder part is taken as an example to demonstrate the use of FEA in the mechanical design. The middle position of the shoulder part is the utmost pressure-point. To sustain the extensive load, a brass rod is used to provide an additional support to this fragile portion. Due to the deflection under operating loads, the maximum displacement of the rod end is approximately 9.44×10^{-3} mm, which is acceptable in experiments. For both components, since the yield strength is two orders of magnitude larger than the maximum of von Mises stress, the design of structure components is reasonable.

Chapter 3

Simulation Studies of a Quadruped Robot

Simulation studies of a quadruped robot motion control system are illustrated in this chapter, including modeling for a robotic leg and the animated simulation. Since the quadrupedal locomotion is implemented by controlling the postures of four legs, the leg model plays an essential role in the motion control system. The leg model needs to be analyzed mathematically, facilitating the controller design to track the desired trajectory. To solve this tracking problem, kinematic and dynamic models of the leg are derived in light of the work in [51]. Two links kinematic conversion is calculated between the foot-end trajectory and joint angles. The dynamic model is implemented to compute the relationship of the actuating torques and joint angles.

After analyzing the leg model, the collaboration of four robotic legs is developed for the quadrupedal locomotion. By setting various footfall patterns, different kinds of gaits can be performed. A four-beat gait has been defined based on the legged motion analysis in [52]. One step cycle of the designed gait is divided into the swing and stance phases. In the swing phase, the contact schedule is associated to the creeping gait and predefined in Section 3.2.1. In the stance phase, the footholds are maintained while shifting the body part forward.

PD control is applied for each joint to operate the leg posture. The corresponding actuating torques are computed to manipulate the foot-ends to realize path following. Moreover, the segment of the desired trajectory of the foot-end in the swing phase fits a fifth order polynomial (results in relatively smooth accelerations). A CAD robot model is converted into MATLAB to animate the quadrupedal locomotion.

Simulation results are demonstrated to analyze the tracking performance in the joint angles and foot-ends.

3.1 Modeling for a Robotic Leg

Since the configurations of four legs are similar, the right front leg model is analyzed as an example, which is shown in Figure 3.1. The robotic leg consists of a set of links connected by joints. Kinematic models and Euler-Lagrange equations are formulated for the robotic leg in this section. By using kinematic equations, the foot-end trajectory and joint angles can be converted to each other. The set of singular configurations is not included in the desired trajectory by calculating the singularities of the Jacobian matrix. Euler-Lagrange equations are implemented to compute the actual angular positions based on the joint torques in the MATLAB/SimMechanics quadruped model.

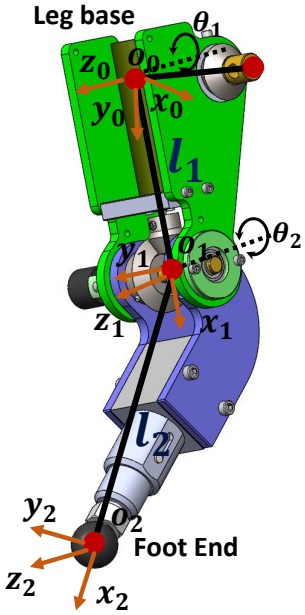

Figure 3.1: Diagram of one leg with relative coordinates for each joint.

3.1.1 Forward Kinematics

Forward kinematic equations are applied in the leg model to compute the joint angles based on the foot-end trajectories. A set of conventions has been developed to

provide a systematic way for this analysis. The Denavi-Hartenberg (DH) convention is implemented in this two-link model, according to [51].

In the leg model, two revolute joints are taken into consideration, and the prismatic joint in the limb part is not considered. The rotations of the hip and knee joints in the lateral plane manipulate the quadruped robot to move forward and backward. The movement direction is maintained which is controlled by rotating the hip joint in the frontal plane. Since we only consider the rectilinear translation in this thesis, the rotation of the hip joint in the frontal plane is not taken into consideration. Besides, joint friction is ignored in the quadruped model. The frame of the foot-end (the tool frame) is fixed based on DH coordinate frame assumptions [51]. By the DH convention, there exists a unique homogeneous transformation matrix A_i that takes the coordinates from the base frame $o_{i-1}x_{i-1}y_{i-1}z_{i-1}$ to the tool frame $o_ix_iy_iz_i$. This matrix A_i is depicted as a product of four basic transformation matrices

$$
\begin{aligned}
A_i =& Rot_{z,\theta_i} Trans_{z,d_i} Trans_{x,l_i} Rot_{x,\alpha_i} \\
=& \begin{bmatrix} c_{\theta_i} & -s_{\theta_i} & 0 & 0 \\ s_{\theta_i} & c_{\theta_i} & 0 & 0 \\ 0 & 0 & 1 & 0 \\ 0 & 0 & 0 & 1 \end{bmatrix} \begin{bmatrix} 1 & 0 & 0 & 0 \\ 0 & 1 & 0 & 0 \\ 0 & 0 & 1 & d_i \\ 0 & 0 & 0 & 1 \end{bmatrix} \begin{bmatrix} 1 & 0 & 0 & l_i \\ 0 & 1 & 0 & 0 \\ 0 & 0 & 1 & 0 \\ 0 & 0 & 0 & 1 \end{bmatrix} \begin{bmatrix} 1 & 0 & 0 & 0 \\ 0 & c_{\alpha_i} & -s_{\alpha_i} & 0 \\ 0 & s_{\alpha_i} & c_{\alpha_i} & 0 \\ 0 & 0 & 0 & 1 \end{bmatrix} \\
=& \begin{bmatrix} c_{\theta_i} & -s_{\theta_i}c_{\alpha_i} & s_{\theta_i}s_{\alpha_i} & a_ic_{\theta_i} \\ s_{\theta_i} & c_{\theta_i}c_{\alpha_i} & -c_{\theta_i}s_{\alpha_i} & a_is_{\theta_i} \\ 0 & s_{\theta_i} & c_{\theta_i} & d_i \\ 0 & 0 & 0 & 1 \end{bmatrix},
\end{aligned} \tag{3.1}
$$

where

$$
Rot_{z,\theta_i} = \begin{bmatrix} c_{\theta_i} & -s_{\theta_i} & 0 & 0 \\ s_{\theta_i} & c_{\theta_i} & 0 & 0 \\ 0 & 0 & 1 & 0 \\ 0 & 0 & 0 & 1 \end{bmatrix}, Trans_{z,d_i} = \begin{bmatrix} 1 & 0 & 0 & 0 \\ 0 & 1 & 0 & 0 \\ 0 & 0 & 1 & d_i \\ 0 & 0 & 0 & 1 \end{bmatrix},
$$

$$
Rot_{x,\alpha_i} = \begin{bmatrix} 1 & 0 & 0 & 0 \\ 0 & c_{\alpha_i} & -s_{\alpha_i} & 0 \\ 0 & s_{\alpha_i} & c_{\alpha_i} & 0 \\ 0 & 0 & 0 & 1 \end{bmatrix}, Trans_{x,l_i} = \begin{bmatrix} 1 & 0 & 0 & l_i \\ 0 & 1 & 0 & 0 \\ 0 & 0 & 1 & 0 \\ 0 & 0 & 0 & 1 \end{bmatrix},
$$

$c_{\theta_i} = \cos\theta_i$, $s_{\theta_i} = \sin\theta_i$, $c_{\alpha_i} = \cos\alpha_i$ and $s_{\alpha_i} = \sin\alpha_i$ according to [51]. In addition, θ_i, l_i, d_i, α_i are parameters associated with the link i and the joint j and denote joint angle, link length, link offset and link twist, respectively. θ_i and α_i are unique angles in the model within a multiple of 2π. θ_i is the joint valuable for a revolute joint, and d_i is the joint valuable for a prismatic joint.

The robotic leg is defined using Cartesian coordinates. The coordinate frames of the leg are depicted in Figure 3.1. The base frame $o_0x_0y_0z_0$ is established at the hip joint of the leg model, where the origin o_0 is located at the middle point of the brass rod between the thigh rails. The $o_1x_1y_1z_1$ frame is fixed at the knee joint, as shown by the DH convention. The origin o_1 is assigned at the middle point of the brass shaft between the knee rails. The tool frame $o_2x_2y_2z_2$ is fixed by setting the origin o_2 at the foot-end. l_1 and l_2 denote the thigh and limb lengths, respectively. The angular positions of the hip and knee joints are θ_1 and θ_2, respectively. The DH parameters are illustrated in Table 3.1.

Table 3.1: Link parameters for the two-link planar leg.

Link Name	a	α	d	θ
Thigh	l_1	0	0	θ_1
Limb	l_2	0	0	θ_2

From (3.1), the A-matrices are given as

$$A_1 = \begin{bmatrix} c_1 & -s_1 & 0 & l_1c_1 \\ s_1 & c_1 & 0 & l_1s_1 \\ 0 & 0 & 1 & 0 \\ 0 & 0 & 0 & 1 \end{bmatrix},$$

where $c_1 = \cos(\theta_1)$ and $s_1 = \sin(\theta_1)$, and

$$A_2 = \begin{bmatrix} c_2 & -s_2 & 0 & l_2c_2 \\ s_2 & c_2 & 0 & l_2s_2 \\ 0 & 0 & 1 & 0 \\ 0 & 0 & 0 & 1 \end{bmatrix},$$

where $c_2 = \cos(\theta_2)$ and $s_2 = \sin(\theta_2)$.

So, the T-matrices can be calculated as follows:

$$
\begin{aligned}
T_1^0 &= A_1 \\
&= \begin{bmatrix} c_1 & -s_1 & 0 & l_1c_1 \\ s_1 & c_1 & 0 & l_1s_1 \\ 0 & 0 & 1 & 0 \\ 0 & 0 & 0 & 1 \end{bmatrix} \\
T_2^0 &= A_1A_2 \\
&= \begin{bmatrix} c_1 & -s_1 & 0 & l_1c_1 \\ s_1 & c_1 & 0 & l_1s_1 \\ 0 & 0 & 1 & 0 \\ 0 & 0 & 0 & 1 \end{bmatrix} \begin{bmatrix} c_2 & -s_2 & 0 & l_2c_2 \\ s_2 & c_2 & 0 & l_2s_2 \\ 0 & 0 & 1 & 0 \\ 0 & 0 & 0 & 1 \end{bmatrix} \\
&= \begin{bmatrix} c_{12} & -s_{12} & 0 & l_1c_1 + l_2c_{12} \\ s_{12} & c_{12} & 0 & l_1s_1 + l_2s_{12} \\ 0 & 0 & 1 & 0 \\ 0 & 0 & 0 & 1 \end{bmatrix},
\end{aligned}
$$

where $c_{12} = \cos(\theta_1 + \theta_2)$ and $s_{12} = \sin(\theta_1 + \theta_2)$. The first two entries of the last column of T_2^0 are the x and y coordinates of the foot-end in the base frame, and they are defined as

$$
\begin{aligned}
x &= l_1c_1 + l_2c_{12}, \\
y &= l_1s_1 + l_2s_{12}.
\end{aligned} \tag{3.2}
$$

3.1.2 Inverse Kinematics

After obtaining the x and y coordinates in (3.2), we can use inverse kinematics equations in [51] to calculate joint angular positions θ_1 and θ_2. From (3.2), we get

$$
x^2 + y^2 = l_1^2 + l_2^2 + 2l_1l_2c_2. \tag{3.3}
$$

Using the Law of Cosines to solve (3.3) for c_2, we obtain

$$
\begin{aligned}
c_2 &= \frac{x^2 + y^2 - l_1^2 - l_2^2}{2l_1l_2}, \\
s_2 &= \pm\sqrt{1 - c_2^2}.
\end{aligned} \tag{3.4}
$$

The multiple solutions in (3.4) correspond to the "elbow-up" position and "elbow-down" position, respectively. Then, we compute θ_2 by using the two-argument arctangent routine

$$\theta_2 = \text{atan2}(s_2, c_2).$$

This approach ensures that all solutions are found in the proper quadrant.

After finding θ_2, we solve (3.2) for θ_1. Particularly, (3.2) can be rewritten as

$$\begin{aligned} x &= k_1 c_1 - k_2 s_1, \\ y &= k_1 s_1 + k_2 c_1, \end{aligned} \tag{3.5}$$

where

$$\begin{aligned} k_1 &= l_1 + l_2 c_2, \\ k_2 &= l_2 s_2. \end{aligned}$$

In order to solve (3.5), r and γ are defined as

$$r = \sqrt{k_1^2 + k_2^2},$$

and

$$\gamma = \text{atan2}(k_2, k_1).$$

Then, we have the following results

$$\begin{aligned} k_1 &= r\cos\gamma, \\ k_2 &= r\sin\gamma. \end{aligned} \tag{3.6}$$

By substituting (3.6) into (3.5), we get

$$\begin{aligned} \frac{x}{r} &= \cos\gamma\cos\theta_1 - \sin\gamma\sin\theta_1, \\ \frac{y}{r} &= \cos\gamma\sin\theta_1 + \sin\gamma\cos\theta_1, \end{aligned}$$

or equivalently,

$$\begin{aligned} \cos(\gamma + \theta_1) &= \frac{x}{r}, \\ \sin(\gamma + \theta_1) &= \frac{y}{r}. \end{aligned}$$

By applying the two-argument arctangent, we get

$$\gamma + \theta_1 = \text{atan2}\left(\frac{y}{r}, \frac{x}{r}\right) = \text{atan2}(y, x).$$

Hence,

$$\theta_1 = \text{atan2}(y, x) - \text{atan2}(k_2, k_1). \tag{3.7}$$

Substituting (3.6) into (3.7), we obtain

$$\theta_1 = \text{atan2}(y, x) - \text{atan2}(l_2 s_2, l_1 + l_2 c_2). \tag{3.8}$$

Note that in (3.4), the sign of s_2 determines the value of k_2, thereby influencing the value of θ_1 according to (3.8). These two solutions correspond to two different postures of the leg. The angular position of the hip joint (θ_1) and knee joint (θ_2) can be computed based on the related parameters, such as the desired position and link length. In summary, forward and inverse kinematics can realize mutual transformation between the foot-end trajectory and joint angular positions.

3.1.3 Jacobian Matrix and the Singularities

To identify a set of singular configurations in the leg movement, the singularities of the Jacobian matrix are calculated. By avoiding the singular configurations in the desired trajectory, the movement direction of the foot-end is arbitrary. Hence, the leg can swing freely to track the desired trajectory of the foot-end.

According to the model of a two-link planar manipulator in [51], the Jacobian matrix is a 6×2 matrix and can be defined as

$$J(\theta) = \begin{bmatrix} z_0 \times (o_2 - o_0) & z_1 \times (o_2 - o_1) \\ z_0 & z_1 \end{bmatrix}, \tag{3.9}$$

where $z_0 \times (o_2 - o_0)$ denotes the vector cross product and

$$o_0 = \begin{bmatrix} 0 \\ 0 \\ o \end{bmatrix}, o_1 = \begin{bmatrix} l_1 c_1 \\ l_1 s_1 \\ o \end{bmatrix}, o_2 = \begin{bmatrix} l_1 c_1 + l_2 c_{12} \\ l_1 c_1 + l_2 s_{12} \\ o \end{bmatrix}, z_0 = z_1 = \begin{bmatrix} 0 \\ 0 \\ 1 \end{bmatrix}.$$

Then, (3.9) can be rewritten as

$$J(\theta) = \begin{bmatrix} J_v \\ J_w \end{bmatrix} = \begin{bmatrix} -l_1 s_1 - l_2 s_{12} & -l_2 s_{12} \\ l_1 c_1 + l_2 c_{12} & l_2 c_{12} \\ 0 & 0 \\ 0 & 0 \\ 0 & 0 \\ 1 & 1 \end{bmatrix}, \tag{3.10}$$

where $J_v = \begin{bmatrix} -l_1 s_1 - l_2 s_{12} & -l_2 s_{12} \\ l_1 c_1 + l_2 c_{12} & l_2 c_{12} \\ 0 & 0 \end{bmatrix}$ and $J_w = \begin{bmatrix} 0 & 0 \\ 0 & 0 \\ 1 & 1 \end{bmatrix}$. For the two-link planar leg, the Jacobian matrix in the frame $o_0 x_0 y_0$ can be represented as

$$J^\circ = \begin{bmatrix} -l_1 s_1 - l_2 s_{12} & -l_2 s_{12} \\ l_1 c_1 + l_2 c_{12} & l_2 c_{12} \end{bmatrix}.$$

Then, we start to calculate kinematic singularities of J°. The set of singular configurations of the leg model satisfies $\det(J^\circ) = 0$. Moreover, the set of singular configurations is computed as $\theta_2 = \pm\pi$. The results mean that the end-effector do not have the velocity along the x_1-axis in singular configurations. Substituting $\theta_2 = \pm\pi$ into (3.10) yields the singularities of $J^\circ_{v_2}$

$$J^\circ_{v_2} = \begin{bmatrix} -l_1 s_1 + l_2 s_1 & +l_2 s_1 \\ l_1 c_1 - l_2 c_1 & -l_2 c_1 \\ 0 & 0 \end{bmatrix}$$

and

$$J^\circ_{v_2} = \begin{bmatrix} -l_1 s_1 - l_2 s_1 & -l_2 s_1 \\ l_1 c_1 + l_2 c_1 & +l_2 c_1 \\ 0 & 0 \end{bmatrix}.$$

Hence, the foot-end can be controlled to move in an arbitrary direction generally. However, when $\theta_2 = \pm\pi$, the foot-end can only move in two specified directions which are vertical to the limb link.

3.1.4 The Euler-Lagrange Equations

By using the Euler-Lagrangian equations in the MATLAB/SimMechancis quadruped model, the actual angular positions can be computed based on the actuating torques of the hip and knee joints. In the leg model, v_{o_1} and v_{o_2} denote the linear velocities for the origin of $o_1x_1y_1z_1$ frame and for the origin of $o_2x_2y_2z_2$ frame, respectively. The kinetic energy $\mathcal{K}$ can be given as

$$\mathcal{K} = \frac{1}{6}m_{l_1}v_{o_1}^T v_{o_1} + \frac{1}{6}m_{l_2}v_{o_2}^T v_{o_2},$$

where m_{l_1} and m_{l_2} denote the mass of the thigh and limb links, respectively. Besides, the potential energy $\mathcal{P}$ due to gravity can be represented as

$$\mathcal{P} = m_{l_1}gh_1 + m_{l_2}gh_2,$$

where $h_1 = c_{12}l_2 + c_1\frac{l_1}{2}$ and $h_2 = c_{12}\frac{l_2}{2}$. h_1 and h_2 denote the heights of the center of gravity for thigh and limb links, respectively. The center of mass is located in the geometric center of each link, which means the distance from the origins in the thigh and knee joints to the center of masses of links are $\frac{l_1}{2}$ and $\frac{l_2}{2}$, respectively. The Lagrangian of the system, $\mathcal{L}$ is given by

$$\begin{aligned}\mathcal{L} =& \mathcal{K} - \mathcal{P} \\ =& \frac{1}{6}m_{l_1}v_{o_1}^T v_{o_1} + \frac{1}{6}m_{l_2}v_{o_2}^T v_{o_2} - (m_{l_2}gh_2 + m_{l_1}gh_1).\end{aligned} \tag{3.11}$$

The orientation of the frame $o_1x_1y_1z_1$ with respect to the frame $o_0x_0y_0z_0$ is

$$o_0o_1 = \begin{bmatrix} l_1c_1 \\ l_1s_1 \\ 0 \end{bmatrix},$$

where o_0 and o_1 are the origins of the base and tool frames in the thigh and knee joints, respectively. Then, we take the derivation for (3.11), the velocity v_{o_1} at the

origin o_1 relative to the base frame $o_0x_0y_0z_0$ is given as

$$v_{o_1} = \begin{bmatrix} -l_1 s_1 \dot{\theta}_1 \\ l_1 c_1 \dot{\theta}_1 \\ 0 \end{bmatrix},$$

We also get

$$v_{o_1}^T v_{o_1} = l_1^2 \dot{\theta}_1^{\,2}. \tag{3.12}$$

The orientation of the frame $o_2x_2y_2z_2$ with respect to the frame $o_0x_0y_0z_0$ is

$$o_0o_2 = \begin{bmatrix} l_1 c_1 + l_2 c_{12} \\ l_1 s_1 + l_2 s_{12} \\ 0 \end{bmatrix}.$$

Similarly, the velocity v_{o_2} at the origin o_2 relative to the base frame $o_0x_0y_0z_0$ is depicted as

$$v_{o_2} = \begin{bmatrix} -l_1 s_1 \dot{\theta}_1 - l_2 s_{12}(\dot{\theta}_1 + \dot{\theta}_2) \\ l_1 c_1 \dot{\theta}_1 + l_2 c_{12}(\dot{\theta}_1 + \dot{\theta}_2) \\ 0 \end{bmatrix}.$$

We also get

$$v_{o_2}^T v_{o_2} = (l_1^2 + 2l_1 l_2 c_2 + l_2^2)\dot{\theta}_1^{\,2} + (2l_1 l_2 c_2 + 2l_2^2)\dot{\theta}_1\dot{\theta}_2 + l_2^2\dot{\theta}_2^{\,2}. \tag{3.13}$$

Then, we substitute (3.12) and (3.13) into (3.11) to obtain

$$\begin{aligned} \mathcal{L}(\theta, \dot{\theta}) =& \frac{1}{6} m_1 l_1^2 \theta_1^2 + \frac{1}{6} m_2 (l_1^2 + 2l_1 l_2 c_2 + l_2^2)\dot{\theta}_1^{\,2} + \frac{1}{3} m_2 (l_1 l_2 c_2 + l_2^2)\theta_1\theta_2 \\ &+ \frac{1}{6} m_2 l_2^2 \dot{\theta}_2^{\,2} - (m_1 g \frac{l_1}{2} c_1 + (m_1 g l_2 + m_2 g \frac{l_2}{2}) c_{12}). \end{aligned} \tag{3.14}$$

The Euler-Lagrange equation is

$$\frac{d}{dt}(\frac{\partial \mathcal{L}}{\partial \dot{\theta}}) - \frac{\partial \mathcal{L}}{\partial \theta} = \tau,$$

where $\tau = \begin{bmatrix} \tau_1 \\ \tau_2 \end{bmatrix}$ and $\theta = \begin{bmatrix} \theta_1 \\ \theta_2 \end{bmatrix}$. τ_1 and τ_2 denote the torques of the hip and knee

joints, respectively. It can also be described as

$$\begin{bmatrix} \frac{d}{dt}(\frac{\partial \mathcal{L}}{\partial \dot{\theta_1}}) \\ \frac{d}{dt}(\frac{\partial \mathcal{L}}{\partial \dot{\theta_2}}) \end{bmatrix} - \begin{bmatrix} \frac{\partial \mathcal{L}}{\partial \theta_1} \\ \frac{\partial \mathcal{L}}{\partial \theta_2} \end{bmatrix} = \begin{bmatrix} \tau_1 \\ \tau_2 \end{bmatrix}, \tag{3.15}$$

where $\frac{\partial \mathcal{L}}{\partial \dot{\theta}} = \begin{bmatrix} \frac{\partial \mathcal{L}}{\partial \dot{\theta_1}} \\ \frac{\partial \mathcal{L}}{\partial \dot{\theta_2}} \end{bmatrix}$, $\frac{d}{dt}(\frac{\partial \mathcal{L}}{\partial \dot{\theta}}) = \begin{bmatrix} \frac{d}{dt}(\frac{\partial \mathcal{L}}{\partial \dot{\theta_1}}) \\ \frac{d}{dt}(\frac{\partial \mathcal{L}}{\partial \dot{\theta_2}}) \end{bmatrix}$ and $\frac{\partial \mathcal{L}}{\partial \theta} = \begin{bmatrix} \frac{\partial \mathcal{L}}{\partial \theta_1} \\ \frac{\partial \mathcal{L}}{\partial \theta_2} \end{bmatrix}$. The elements in (3.15) are calculated and presented as

$$\begin{aligned}
\frac{\partial \mathcal{L}}{\partial \dot{\theta_1}} =& \frac{1}{3} m_1 l_1^2 \dot{\theta_1} + \frac{1}{3} m_2 (l_1^2 + 2 l_1 l_2 c_2 + l_2^2) \dot{\theta_1} + \frac{1}{3} m_2 (l_1 l_2 c_2 + l_2^2) \dot{\theta_2}, \\
\frac{\partial \mathcal{L}}{\partial \dot{\theta_2}} =& \frac{1}{3} m_2 (l_1 l_2 c_2 + l_2^2) \dot{\theta_1} + \frac{1}{3} m_2 l_2^2 \dot{\theta_2}, \\
\frac{\partial \mathcal{L}}{\partial \theta_1} =& m_1 g \frac{l_1}{2} s_1 + (m_1 l_2 + m_2 \frac{l_2}{2}) g s_{12}, \\
\frac{\partial \mathcal{L}}{\partial \theta_2} =& (m_1 l_2 + m_2 \frac{l_2}{2}) g s_{12} - \frac{1}{3} m_2 l_1 l_2 \dot{\theta_1}^2 s_1 - \frac{1}{3} m_2 l_1 l_2 \dot{\theta_1} \dot{\theta_2} s_2, \\
\frac{d}{dt}(\frac{\partial \mathcal{L}}{\partial \dot{\theta_1}}) =& (\frac{1}{3} m_1 l_1^2 + \frac{1}{3} m_2 (l_1^2 + 2 l_1 l_2 c_2 + l_2^2)) \ddot{\theta_1} + \frac{1}{3} m_2 (l_1 l_2 c_2 + l_2^2) \ddot{\theta_2} \\
& - \frac{2}{3} m_2 l_1 l_2 s_2 \dot{\theta_1} \dot{\theta_2} - \frac{1}{3} m_2 l_2 s_2 \dot{\theta_2}^2, \\
\frac{d}{dt}(\frac{\partial \mathcal{L}}{\partial \dot{\theta_2}}) =& \frac{1}{3} m_2 (l_1 l_2 c_2 + l_2^2)) \ddot{\theta_1} + \frac{1}{3} m_2 l_2^2 \ddot{\theta_2} - \frac{1}{3} m_2 l_1 l_2 s_2 \dot{\theta_1} \dot{\theta_2}.
\end{aligned}$$

Substituting above equations into (3.15) yields

$$\begin{bmatrix} \frac{1}{3} m_1 l_1^2 + \frac{1}{3} m_2 (l_1^2 + 2 l_1 l_2 c_2 + l_2^2) & \frac{1}{3} m_2 (l_1 l_2 c_2 + l_2^2) \\ \frac{1}{3} m_2 (l_1 l_2 c_2 + l_2^2) & \frac{1}{3} m_2 l_2^2 \end{bmatrix} \begin{bmatrix} \ddot{\theta}_1 \\ \ddot{\theta}_2 \end{bmatrix}$$
$$+ \begin{bmatrix} -\frac{2}{3} m_2 l_1 l_2 s_2 \dot{\theta_2} & -\frac{1}{3} m_2 l_1 l_2 s_2 \dot{\theta_2} \\ \frac{1}{3} m_2 l_1 l_2 s_1 \dot{\theta_1} & 0 \end{bmatrix} \begin{bmatrix} \dot{\theta}_1 \\ \dot{\theta}_2 \end{bmatrix} + \begin{bmatrix} -m_1 g \frac{l_1}{2} s_1 - (m_1 g l_2 + m_2 g \frac{l_2}{2}) s_{12} \\ -(m_1 g l_2 + m_2 g \frac{l_2}{2}) s_{12}. \end{bmatrix} = \begin{bmatrix} \tau_1 \\ \tau_2 \end{bmatrix}. \tag{3.16}$$

Moreover, (3.16) can be represented as

$$D(\theta)\ddot{\theta} + C(\theta, \dot{\theta})\dot{\theta} + G(\theta) = \tau, \tag{3.17}$$

where

$$D(\theta) = \begin{bmatrix} \frac{1}{3}m_1 l_1^2 + \frac{1}{3}m_2(l_1^2 + 2l_1 l_2 c_2 + l_2^2) & \frac{1}{3}m_2(l_1 l_2 c_2 + l_2^2) \\ \frac{1}{3}m_2(l_1 l_2 c_2 + l_2^2) & \frac{1}{3}m_2 l_2^2 \end{bmatrix},$$

$$C(\theta, \dot{\theta}) = \begin{bmatrix} -\frac{2}{3}m_2 l_1 l_2 s_2 \dot{\theta}_2 & -\frac{1}{3}m_2 l_1 l_2 s_2 \dot{\theta}_2 \\ \frac{1}{3}m_2 l_1 l_2 s_1 \dot{\theta}_1 & 0 \end{bmatrix},$$

$$G(\theta) = \begin{bmatrix} -m_1 g \frac{l_1}{2} s_1 - (m_1 g l_2 + m_2 g \frac{l_2}{2}) s_{12} \\ -(m_1 g l_2 + m_2 g \frac{l_2}{2}) s_{12} \end{bmatrix},$$

and $\tau = \begin{bmatrix} \tau_1 \\ \tau_2 \end{bmatrix}$, $\ddot{\theta} = \begin{bmatrix} \ddot{\theta}_1 \\ \ddot{\theta}_2 \end{bmatrix}$, $\dot{\theta} = \begin{bmatrix} \dot{\theta}_1 \\ \dot{\theta}_2 \end{bmatrix}$. $D(\theta)$ is the mass-inertia matrix, $C(\theta, \dot{\theta})$ is the matrix of centripetal and Coriolis terms, and $G(\theta)$ is the gravity vector. By utilizing (3.17), the actual angular positions can be calculated in the MATLAB/SimMechanics quadruped model based on the joint torques.

3.2 Animated Simulation

An animated simulation is developed to analyze the tracking performance in the quadrupedal locomotion. First, the movement of four legs are assigned in a sequence based on a proper gait. Then, PD control is implemented to manipulate the leg posture to execute the locomotion, according to the designed trajectories. Based on a simplified CAD model, a SimMechanics quadruped model is established to emulate the motion of the robot. Relative simulation results are also analyzed.

3.2.1 Gait Selection

An appropriate gait is selected to emulate the quadrupedal locomotion by comparing different gaits. In [14], quadruped gaits are classified into the two-beat gait and the four-beat gait, as shown in Figure 3.2. The two-beat gait can be subdivided into the pacing (see Figure 3.2a) and trotting gaits (see Figure 3.2b). In the two-beat gait, four feet are assigned into two groups. Two feet in either group are designed to touch the ground synchronously. When the feet strike the ground, identical forces will act on hip joints. Theoretically, since no extra torque is transmitted to the other side of the body part, no vertical vibration is caused in the body.

For each step, the balance footholds are defined as the location on the terrain where

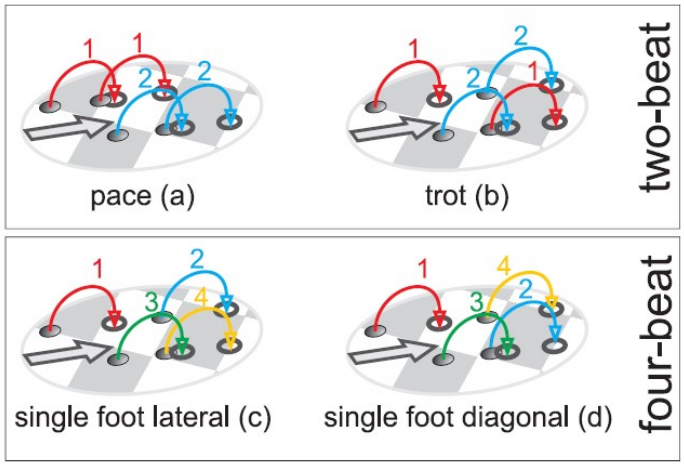

Figure 3.2: Classification of periodic gaits [14].

the feet should be placed to continue balanced steady-state locomotion. Compared to the two-beat gait, the four-beat gait provides more choices of footholds in rough terrain. Hence, with respect to the available footholds on the ground, the placement of the feet can interact with the stability and general behavior of the quadruped robot. For the single foot lateral gait (see Figure 3.2c) and the single foot diagonal gait (Figure 3.2d), the foot-ends strike the ground in a symmetric footfall sequence. In both of these four-beat gaits, triple feet touch the ground alternately at the same time. To maintain stability in the locomotion, the projected center of gravity lies within the support polygon, which is defined by the footholds [1].

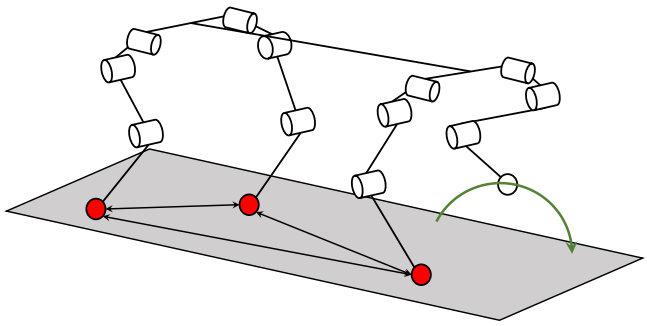

Figure 3.3: Internal contact directions of the creeping gait.

Several typical kinds of gaits are described in the following. The pacing, trotting and bounding gaits are two-beat gaits. The creeping and tölting gaits are four-beat gaits.

- In the pacing gait, lateral pairs of legs move synchronously. The pacing gait is appropriate for the quadruped robot to execute a high-speed locomotion on flat ground.
- In the trotting gait, diagonal pairs of legs move at the same time. Its energy consumption is relatively low at a high-speed motion.
- In the bounding gait, the front pair of legs and hind pair of legs move in sequence.
- In the creeping gait, as shown in Figure 3.4, the quadruped robot continuously executes the footfall pattern LH, LF, RH, and RF in a lateral footfall sequence [52]. The abbreviations stand for left hind (LH), left fore (LF), right hind (RH) and right fore (RF). In this static gait, triple feet alternately provide the support. Since its energy cost is relatively low at a low-speed motion, this gait is appropriate for traversing rocky and sloped terrain.
- The tölting gait is extracted from the locomotion performance of icelandic horses in [53]. The tölting gait has the same footfall sequence as the creeping gait. But the touch-down phase of the tölting gait occupies less percentage in one step cycle than the creeping gait. Consequently, a single foot and double feet alternately provide the support.

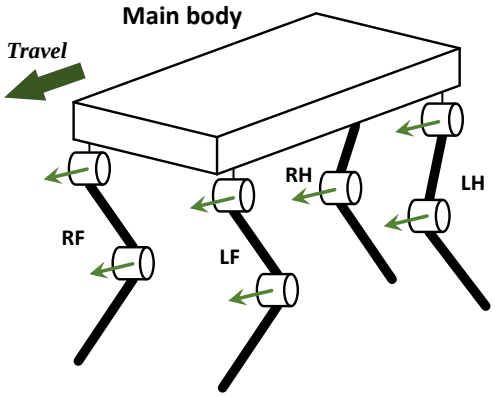

Figure 3.4: The schematic model of a quadruped system.

Generally, various kinds of gaits have their own advantages in different environments in [54]. The creeping gait is a suitable choice for the quadruped robot in a low speed motion. Since triple feet alternately provide the support in the locomotion, this four-beat gait presents high stability. In addition, the energy cost of the creeping gait is lower than other gaits at a low-speed motion. Hence, the creeping gait is chosen to be applied in the designed robot. Figure 3.3 shows internal contact directions in the creeping gait.

As one type of four-beat gaits, the creeping gait is selected to perform the low-speed locomotion due to its low energy consumption and substantial available footholds. In the creeping gait, the predefined footfall pattern is (LH→ LF→ RH → RF → LH→...), and this sequence can be readily generated in MATLAB. A step cycle of the quadrupedal locomotion can be divided into the swing and stance phases according to [52]. Figure 3.5 shows that the sequence of swing and stance phases for a one-legged robot is separated by a short moment called toe-off in [15].

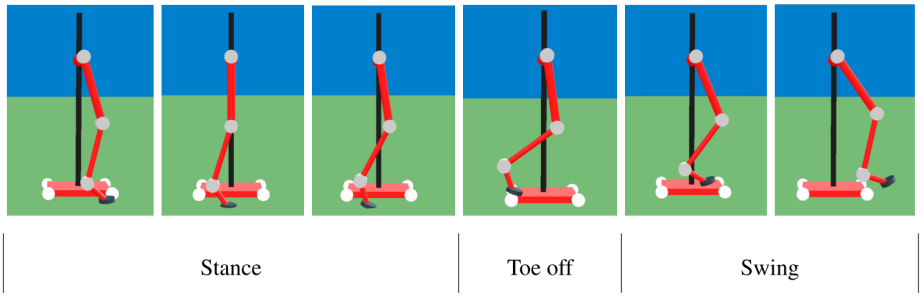

Figure 3.5: Sequence of the locomotion cycle simulation in [15].

3.2.2 PD Control

To manipulate the leg posture to execute the locomotion, each joint is operated by the PD controller. Figure 3.6 shows the block diagram of a quadruped robot motion control system. The desired trajectories of foot-ends are formed based on the footfall sequence of the creeping gait, and the desired angular positions for the hip and knee joints can be calculated by using inverse kinematics equations. For each joint, the control signal is calculated by a PD controller based on the difference between the desired and actual angular positions. By importing the control signal to the ideal motor block, the joint torque is generated to manipulate the leg posture, thereby executing the quadrupedal locomotion. In the MATLAB/SimMechanics model, the

actual angular positions of hip and knee joints are computed based on (3.17). Many physical effects are ignored in this simplified model.

For each joint, a PD controller is applied to make the response to meet the design specifications, as shown in the area of the orange dotted lines in Figure 3.4. Based on the error value of angular positions, the proportional and derivative gains are implemented to generate the actuating torques. To set up the parameters of the PD controller, the proportional gain K_p is adjusted firstly. K_p is proportional to the current value of the error $\Delta\theta = \theta - \theta_d$, where θ and θ_d denote the actual joint angle and the desired joint angle, respectively. Then, to reduce the effect of the error, the derivative gain K_d is used to exert the control influence, which is generated by the rate of error change. After several tests, the appropriate K_p and K_d for the hip joint are chosen as 20 and 2, respectively. K_p and K_d for the knee joint are selected as 10 and 1, respectively. Similarly, by applying the PD controller, the control signal for the motor in the knee joint is generated to actuate the limb link. Meanwhile, the PD controller in the hip joint provides the control signal to the ideal motor block to actuate the whole leg, which is twice the mass of the limb. Hence, it is reasonable that PD parameters for the hip joint are twice as parameters for the knee joint. Since the residual error in the system is relatively small and no need to be eliminated, the integral term is not added in the controller. The details of the trajectory generator and SimMechanics quadruped model in Figure 3.6 are illustrated in Section 3.2.3 and 3.2.4.

3.2.3 Generating Smooth Trajectories

Based on the above investigation of gait selection, the creeping gait is implemented for the quadrupedal locomotion. In this gait, triple and quadruple legs alternatively provide the support to the robot. The quadrupedal locomotion can be divided into the swing and stance phases. In the swing phase, four legs swing forward in the predefined sequence while other three legs go through a rest period to provide the support. In the stance phase, the foot-ends are supposed to connect the ground with a complete stop, and the legs move synchronously to shift the main body forward.

The foot-ends are modeled as points without geometrical extension. In the stance phase, the foot-ends are modeled as simple rotational joints, which connect the legs as fixed points on the flat terrain. The legs move freely around the hip and knee joints freely, thereby providing a total of three degrees of freedom.

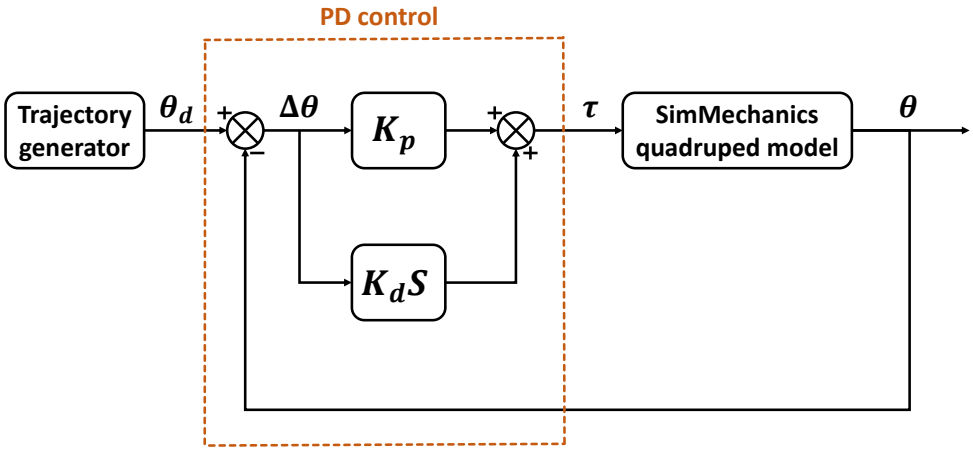

Figure 3.6: PD control schematics.

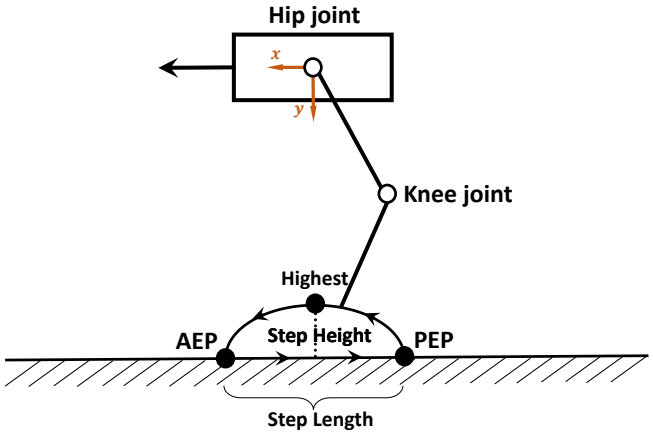

Figure 3.7: Nominal trajectory of the leg.

The desired trajectory of the foot-end is generated based on the movement of the foot-end in the predefined pattern. Also, the desired trajectory is limited by the mechanism of each robotic leg, and the dimensions of one leg are provided in Table 3.2. To move the leg freely without any restrictions, the set of singular configuration $\theta_2 = \pm\pi$ is not included in the desired trajectory. As illustrated in Figure 3.7, three

significant points are selected to form the desired trajectory of the foot end in the swing phase. First of all, the start point of one step cycle is the posterior extreme position (PEP) where the foot-end lifts off the ground. As shown in Figure 3.8, the origin of the base frame is set at the hip joint of the leg, and the PEP is at [-0.051 m, 0.254 m, 0 m]. Then, the leg swings to the highest position. This half-way point of the swing phase is at [0 m, 0.203 m, 0 m]. Finally, the foot-end strikes the ground in the touchdown phase at the anterior extreme position (AEP), which is at [0.051 m, 0.254 m, 0 m]. In addition, two relative points are also chosen to smooth the path around the highest position. These relative points are at [0.036 m, 0.218 m, 0 m] and [0.036 m, 0.218 m, 0 m], respectively. Based on three significant points and two relative points, a fifth order polynomial can be formulated to form each individual spline segment of the desired trajectory.

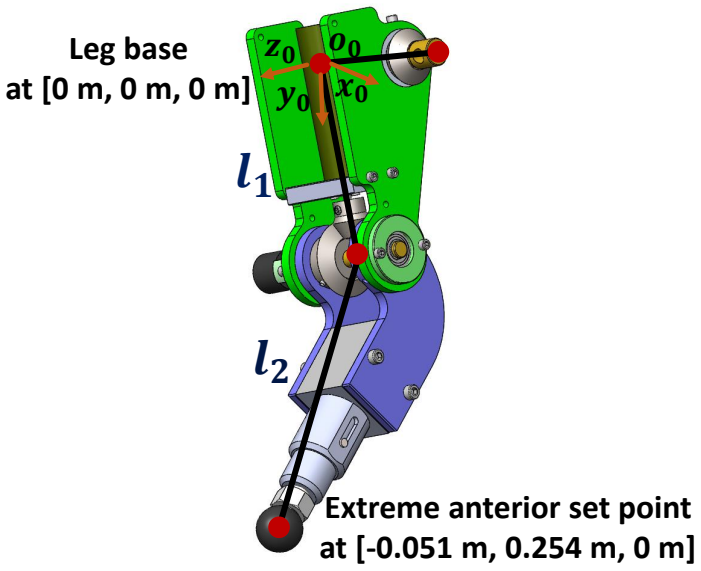

Figure 3.8: A posterior extreme set point for one step shown with Cartesian coordinates.

3.2.4 MATLAB/SimMechanics Model

The designed CAD model in Chapter 2 is too complicated for MATLAB to compute. Hence, a simplified CAD model is developed for an animated simulation, whose main characteristics of the designed robot are maintained, such as the mass and

Table 3.2: Some parameters of the designed quadruped robot.

Link name	**Length (m)**	**Width (m)**	**Thickness (m)**
Thigh	0.152	0.089	0.089
Limb	0.152	0.076	0.076

link length. The LH, LF, RH and RF legs are painted blue, red, green and yellow, as illustrated in Figure 3.9. The simplified CAD model is converted into the MATLAB/SimMechanics model with the help of MATLAB/SimMechanics packages. Related MATLAB/Simulink blocks are also set up to model the dynamics of the quadruped robot. The desired trajectories are generated in MATLAB based on a fifth polynomial. Environment blocks should be carefully set to provide the global information about the workspace, such as the gravitational acceleration and global coordinate system. The gravitational acceleration is set to be 9.81 m/s^2 in the simulation.

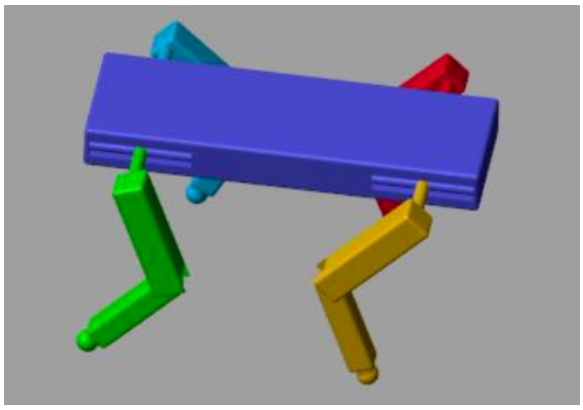

Figure 3.9: The simulated animation for the simplified model.

To set up the MATLAB/SimMechanics quadruped model, the thigh link connects the shoulder and limb links through two revolute joint blocks, which represent the hip and knee joints, respectively. Four shoulder links are rigidly attached to the main body. Other related information is determined by the simplified CAD model, such as the link connection, the link mass and the center of mass for each part.

For the leg model, the origin of the base frame is set at the connection of the shoulder and thigh links. Both the hip and knee joints are designed to rotate about the z-axis in their corresponding base frames. At the beginning of the simulation,

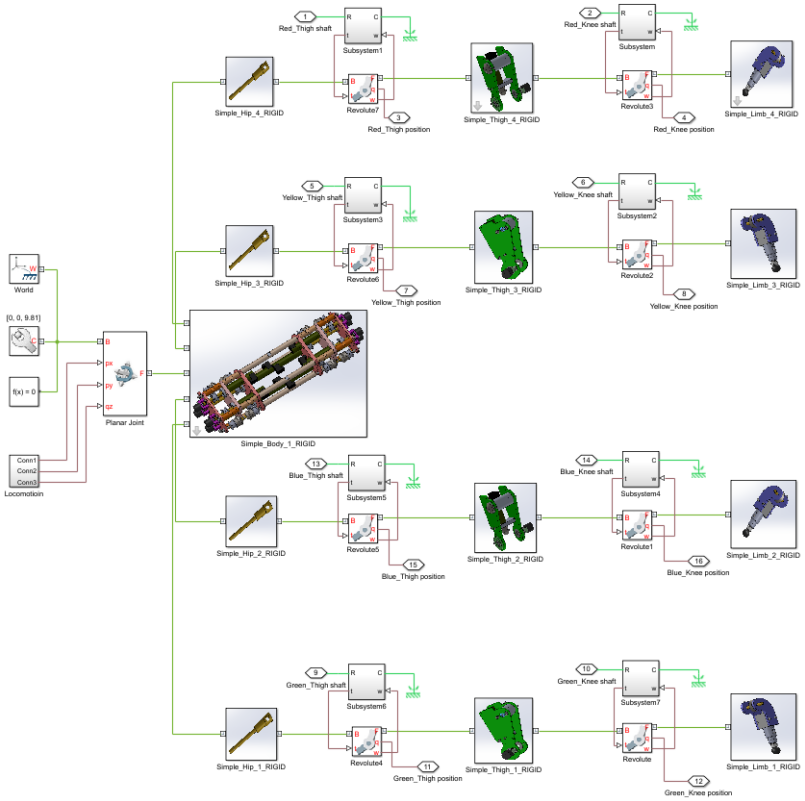

Figure 3.10: The MATLAB/SimMechanics quadruped model.

relative coordinate systems should be initialized in the hip and knee joints and foot-ends, as illustrated in Figure 3.1. In other words, as discussed in Section 3.1, we need to define the transformation matrix from the hip joint to the knee joint, and furthermore, define the transformation matrix from the knee joint to the foot-end. By applying transformation matrices, the directions of axes are re-oriented in the base frames. For example, the knee joint angular position θ_2 of the LF should be initialized as $-\theta_2$ to present the rotation angle. The details of the MATLAB/SimMechanics model are illustrated in Figure 3.10.

3.2.5 Simulation Results

Simulation results are analyzed to demonstrate the effectiveness of the quadruped robot motion control system. By connecting the three critical points and two relative points with a fixed step size 0.001s, the desired trajectories of the foot-ends are generated based on a fifth order polynomial with a shape similar to a sine wave. Then, the desired joint angular positions can be computed by applying inverse kinematics

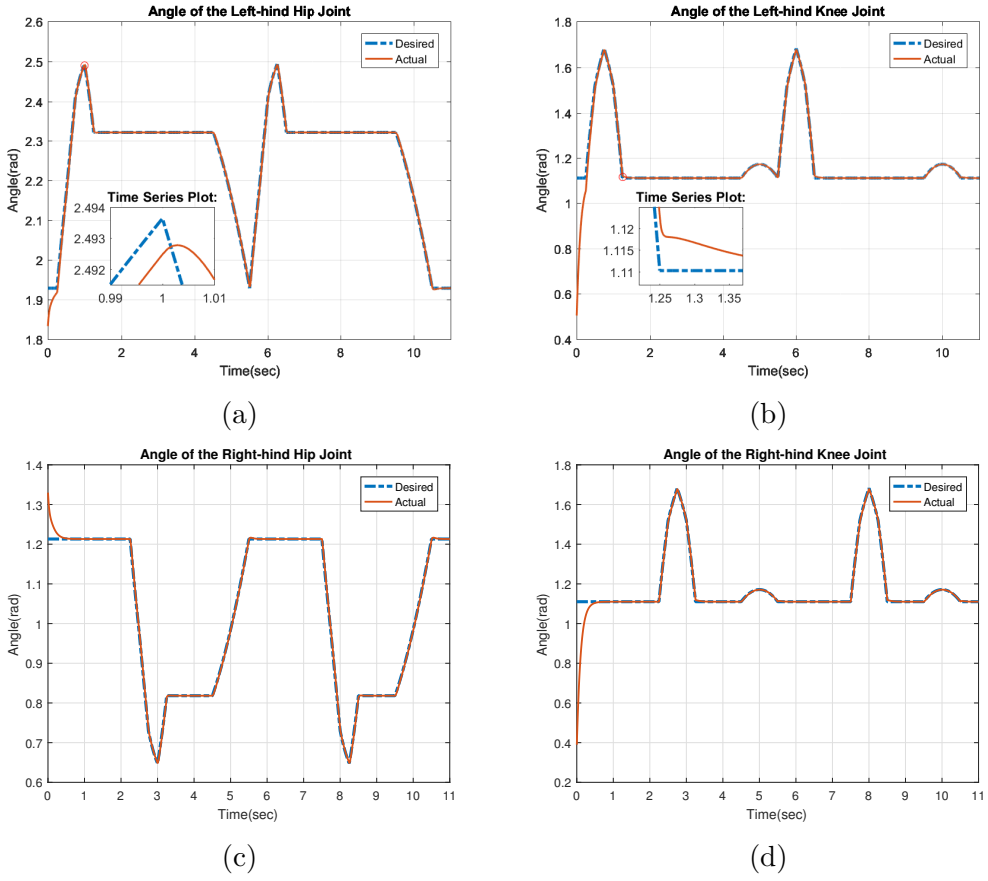

Figure 3.11: Illustrations of the desired and tracked angle of the hip joint and knee joint of hind legs: (a) the left-hind hip joint, (b) left-hind knee joint, (c) right-hind hip joint and (d) right-hind knee joint.

equations. The actuating torques are computed by using PD control based on the desired angular positions. By implementing Euler-Lagrange equations, the actual joint positions are generated, as illustrated in Figure 3.6. The actual trajectories of the foot-ends are further calculated by using forward kinematics equations. In Figure 3.11, Figure 3.12 and Figure 3.13, the blue curves denote the desired trajectories for the joint angles or foot-ends, and the red curves denote the actual trajectories for the joint angles or foot-ends in each case.

We take the left-hind (LH) leg as an example to demonstrate the quadrupedal locomotion in one step cycle as shown in Figure 3.11a and Figure 3.11b. Each step cycle lasts for 5.25 s, and the swing phase is from 0.25 s to 1.25 s. Then, the LH leg goes through a rest period while the other legs are in the swing phase in order. The LH leg is in a stance phase from 4.5 s to 5.5 s. The foot-end lifts off the ground at

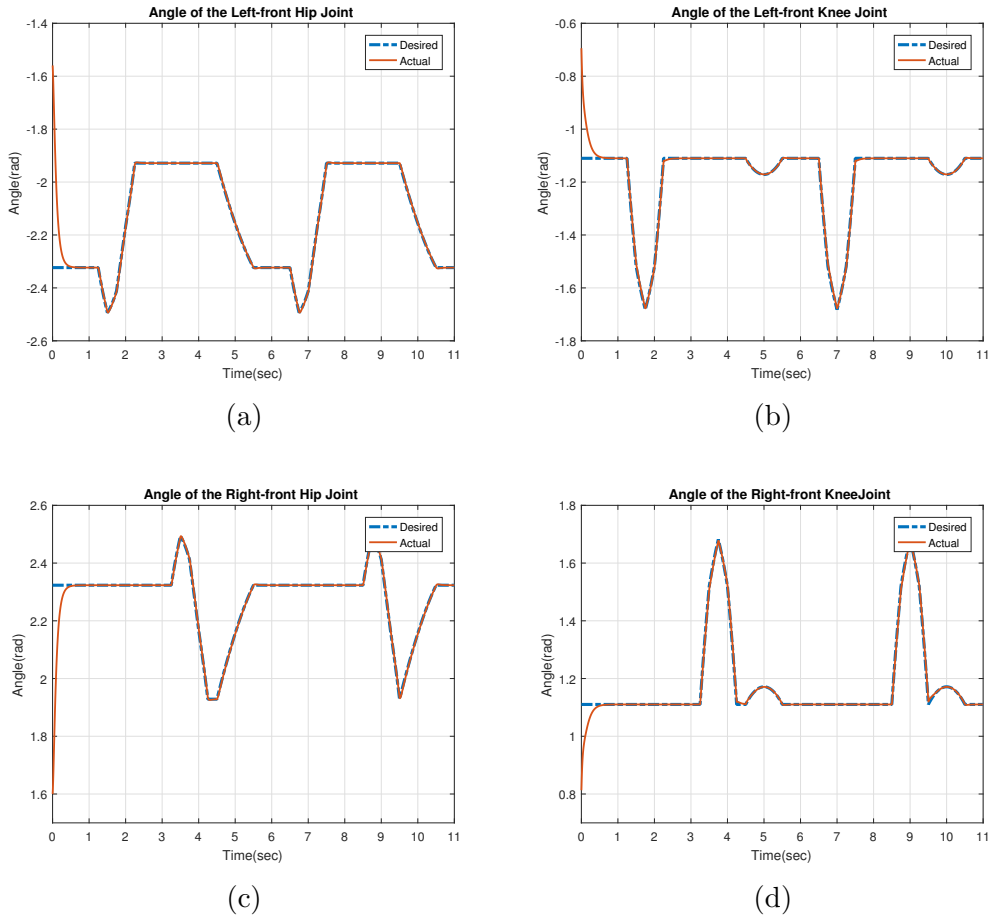

Figure 3.12: Illustrations of the desired and tracked angle of the hip joint and knee joint of front legs: (a) the left-front hip joint, (b) left-front knee joint, (c) right-front hip joint and (d) right-front knee joint.

the PEP of the step cycle to the half-way point, and then touches down at the AEP.

Figure 3.11 and Figure 3.12 demonstrate the tracking performance of the designed motion controller for the hind legs and front legs in two step cycles. The desired and tracked angle trajectories of each joint are illustrated in the subfigures of Figure 3.11 and Figure 3.12. From the simulation results, it can be observed that, at the beginning of the locomotion, it takes around 0.25 s for each joint to track the desired angular position. Then, each joint angle is capable of tracking the desired angular position with an approximately 0.001 rad. The tracking performances around the red circles are illustrated in the time series plots.

The simulation results of foot-end positions in a sequence of LH, LF, RH, and RF are shown in Figure 3.13. At the beginning of the simulation, the foot-end is

controlled to track the initial point of the desired trajectory, so the displacement of the position is relatively large. After around 0.25 s, the foot-end starts to track the desired path in a relatively good condition.

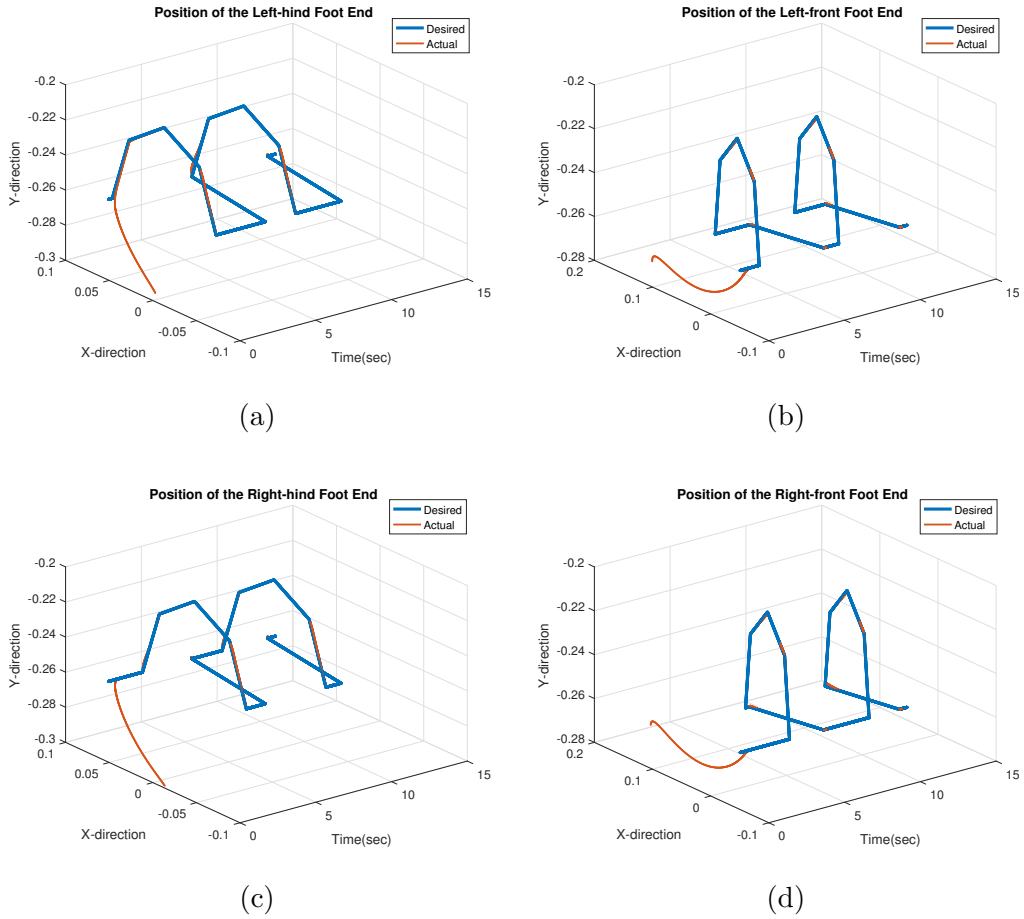

Figure 3.13: Illustrations of the desired and tracked angle of four foot-ends: (a) the left-hind foot-end, (b) left-front foot-end, (c) right-hind foot-end and (d) right-front foot-end.

3.3 Conclusion

In this chapter, we focus on modeling for a robotic leg and the animated simulation of the designed quadruped robot. Forward and inverse kinematics equations are utilized in the leg model, and singularities of the Jacobian matrix is calculated to identify the singular configurations. Then, Euler-Lagrange equations are applied to calculate the hip and knee joint torques, respectively. Furthermore, an animated simulation of the

quadrupedal locomotion is emulated with the creeping gait. The desired trajectories of foot-ends are generated based on the predefined footfall sequence. At last, the MATLAB/SimMechanics model is established in MATLAB. By using PD control to manipulate the joints, the foot-ends track the desired paths well.

Chapter 4

Conclusions and Future Work

4.1 Conclusions

This thesis mainly introduces the mechanical design and simulation studies of a quadruped robot motion control system. An animated simulation of the quadrupedal locomotion has been emulated by combining MATLAB and SolidWorks.

In Chapter 2, the mechanical structure of the quadruped robot is presented. Particularly, section 2.1 introduces some key components, such as DC motors and potentiometers. Additionally, the leg mechanism is optimized to improve the characteristics of the compliant leg, such as the speed, endurance, agility and strength. Several methods are applied to design the robot from the aspects of the leg length, mass distribution, leg kinematics, elastic energy storage and muscle power. To absorb the impact force at collision, linear telescoping joints are incorporated in the limb links to realize the internal energetic conversion. In Section 2.4, the structural components are optimized to enhance the fragile position by using FEA. Besides, structural components in the hip joint are demonstrated as examples in the design process.

In Chapter 3, the modeling for the robotic leg and animated simulation are illustrated. Kinematic and dynamic parameters of the leg model are specified based on a CAD model, which is drawn by SolidWorks. Based on the deviation between the desired and tracked joint angles, the PD control is implemented to generate a PWM signal to actuate the DC motor. Actuated by the joint torques, the hip and knee joints are manipulated to adjust the leg postures. By choosing appropriate footholds, the quadrupedal locomotion is executed in a creeping gait. One step cycle of the quadruped movement is divided into the stance and swing phases. In the stance

phase, the quadruped robot maintains the foothold position while shifting the body part forward. In the swing phase, four legs are controlled to execute the quadrupedal locomotion in the predefined footfall pattern.

4.2 Future Work

In the future, we plan to improve the designed quadruped robot from the perspectives of mechanical design and control strategy. From the aspect of the mechanical design, a higher gear ratio can be applied to improve the leg stiffness in the hip and knee joints. As mentioned in Section 1.2, the robotic leg can be composed of compliant mechanisms, such as the leg of "RHex" [38]. In the limb part, the telescoping joint can be upgraded to PAM with solenoid valves and check valves, such as the 3D one-leg hopping machine [22]. Steel coil springs can also be used to avoid assembling the motor in the thigh part. This mechanism not only reduces the leg weight, but also improves the agility of the leg.

New type actuators are also expected to be assembled in the robot. For example, Maxon EC-4pole brushless motors, which is implemented in "StarlETH" [1], can provide maximal velocity and torque for short-term operation. The ANYdrive in "ANYmal" can be used to actuate the joint directly [55]. Timing belts and gears are no longer to be assembled to redirect the actuating torque. Hence, by applying this type of actuators, the mechanical structure is significantly simplified.

To design an autonomous legged robot, we also plan to work on the control strategy. The overview of the control architecture for the quadrupedal locomotion is illustrated in Figure 4.1. The hierarchical control structure has been divided into the high and low level controls, which are processed by the FPGA and ARM architectures, respectively.

The FPGA is used to conduct the high level control, such as visual image processing and proper gaits selection [1]. The ARM architecture is applied to control the hip and knee joints, thereby manipulating the posture of each leg. Force sensors can be assembled at the foot-ends to measure the slope angle of the connect surface for the quadruped posture adjustment. Cameras can collect the surrounding information, thereby helping the robot to choose the appropriate footholds.

For the high level control, the FPGA is applied with cameras for image processing. Based on the collected data, an updated map can be processed for path planning and obstacle avoidance. The FPGA is used to set up a vision system for inline processing.

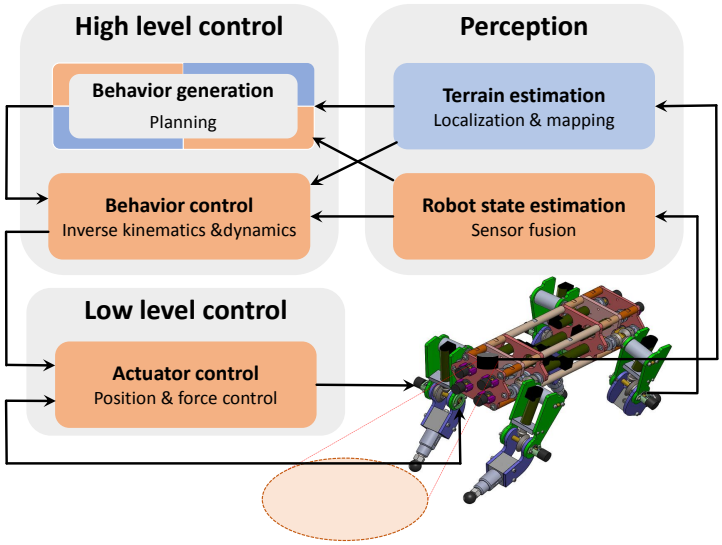

Figure 4.1: An overview of the control architecture for the quadrupedal locomotion.

High-speed control operations can be implemented in the FPGA with short processing time. Proper gaits can also be applied in this architecture according the environmental conditions. For instance, when the terrain is relatively smooth, dynamic gaits can be applied for a high speed locomotion. Otherwise, static gaits is the optimal option, when the robot moves in rough terrain.

For the low level control, the ARM architecture is used to generate the leg trajectory by controlling the joint angles. The stride of one step cycle is adjusted in this level for the dynamically stable legged robot. By controlling the joint angles, the act of positioning the foot-ends interacts with the stability of the quadrupedal locomotion. To balance steady-state mobility, the ARM architecture is applied for positioning the foot-ends in the appropriate locations. The ARM architecture not only can operate the legs touching the ground in the desired footholds, but also can adjust the posture of the robot.

Overall, the hierarchical structure of the path planner is expected to be developed for the designed quadruped robot in the future.

Bibliography

[1] M. Hutter, C. Gehring, M. A. Höpflinger, M. Blösch, and R. Siegwart, "Toward combining speed, efficiency, versatility, and robustness in an autonomous quadruped," *IEEE Trans. Robot.*, vol. 30, no. 6, pp. 1427–1440, 2014.

[2] Boston Dynamics Inc. (2017). [Online]. Available: http://www.bostondynamics.com

[3] S. Seok, A. Wang, M. Y. Chuah, D. Otten, J. Lang, and S. Kim, "Design principles for highly efficient quadrupeds and implementation on the MIT Cheetah robot," in *Proc. IEEE Int. Conf. Robot. Autom.*, Karlsruhe, Germany, May. 2013, pp. 3307–3312.

[4] S. Hirose. (2017). [Online]. Available: http://robotlocomotion.mech.kit.ac.jp/research/Quadruped/photo-movie-pat2-e.html

[5] ——. (2017). [Online]. Available: http://robotlocomotion.mech.kit.ac.jp/research/Quadruped/photo-movie-tekken2-photo.html

[6] M. H. Raibert, H. B. Brown Jr, and M. Chepponis, "Experiments in balance with a 3D one-legged hopping machine," *Int. J. Robot. Res.*, vol. 3, no. 2, pp. 75–92, 1984.

[7] B. Vanderborght, B. Verrelst, R. Van Ham, M. Van Damme, P. Beyl, and D. Lefeber, "Development of a compliance controller to reduce energy consumption for bipedal robots," *Auton. Robots*, vol. 24, no. 4, pp. 419–434, 2008.

[8] R. Niiyama, A. Nagakubo, and Y. Kuniyoshi, "Mowgli: A bipedal jumping and landing robot with an artificial musculoskeletal system," in *Proc. IEEE Int. Conf. Robot. Autom.*, Rome, Italy, Apr. 2007, pp. 2546–2551.

[9] M. Ahmadi and M. Buehler, "Preliminary experiments with an actively tuned passive dynamic running robot," in *Proc. Int. Symp. Exp.*, Barcelona, Spain, Jun. 1998, pp. 312–324.

[10] J. Estremera and K. J. Waldron, "Thrust control, stabilization and energetics of a quadruped running robot," *Int. J. Robot. Res.*, vol. 27, no. 10, pp. 1135–1151, 2008.

[11] K. S. Yamazaki, "The design and control of Scout I, a simple quadruped robot," Ph.D. dissertation, McGill Univ., Montreal, QC, Canada, 1999.

[12] I. Poulakakis, J. A. Smith, and M. Buehler, "Modeling and experiments of untethered quadrupedal running with a bounding gait: The Scout II robot," *Int. J. Robot. Res.*, vol. 24, no. 4, pp. 239–256, 2005.

[13] H. Kimura, Y. Fukuoka, and A. H. Cohen, "Adaptive dynamic walking of a quadruped robot on natural ground based on biological concepts," *Int. J. Robot. Res.*, vol. 26, no. 5, pp. 475–490, 2007.

[14] C. D. Remy, K. Buffinton, and R. Siegwart, "Stability analysis of passive dynamic walking of quadrupeds," *Int. J. Robot. Res.*, vol. 29, no. 9, pp. 1173–1185, 2010.

[15] E. Garcia, J. C. Arevalo, G. Munoz, and P. Gonzalez-de Santos, "On the biomimetic design of agile-robot legs," *Sensors*, vol. 11, no. 12, pp. 11 305–11 334, 2011.

[16] P. G. de Santos, E. Garcia, J. Cobano, and T. Guardabrazo, "Using walking robots for humanitarian de-mining tasks," in *Proc. 35th Int. Symp. Robot.*, Paris, France, Mar. 2004, CD-ROM.

[17] C. S. Sharp, O. Shakernia, and S. Sastry, "A vision system for landing an unmanned aerial vehicle," in *Proc. IEEE Int. Conf. Robot. Autom.*, Seoul, Korea, May. 2001, pp. 1720–1727.

[18] P. Corke, C. Detweiler, M. Dunbabin, M. Hamilton, D. Rus, and I. Vasilescu, "Experiments with underwater robot localization and tracking," in *Proc. IEEE Int. Conf. Robot. Autom.*, Roma, Italy, Apr. 2007, pp. 4556–4561.

[19] J.-F. Lalonde, N. Vandapel, D. F. Huber, and M. Hebert, "Natural terrain classification using three-dimensional ladar data for ground robot mobility," *J. Robot. Syst.*, vol. 23, no. 10, pp. 839–861, 2006.

[20] C. Ridderström, "Legged locomotion: Balance, control and tools-from equation to action," Ph.D. dissertation, Royal Inst. Technol., Stockholm, Sweden, 2003.

[21] K. J. Waldron, V. J. Vohnout, A. Pery, and R. B. McGhee, "Configuration design of the adaptive suspension vehicle," *Int. J. Robot. Res.*, vol. 3, no. 2, pp. 37–48, 1984.

[22] M. H. Raibert, *Legged Robots that Balance*. Cambridge, MA, USA: MIT press, 1986.

[23] M. G. Bekker, *Introduction to Terrain-vehicle Systems*. Ann Arbor, MI, USA: University of Michigan Press, 1969.

[24] P. Gregorio, M. Ahmadi, and M. Buehler, "Design, control, and energetics of an electrically actuated legged robot," *IEEE Trans. Syst., Man Cybern.*, vol. 27, no. 4, pp. 626–634, 1997.

[25] Y. Li, B. Li, J. Ruan, and X. Rong, "Research of mammal bionic quadruped robots: A review," in *Proc. Int. Conf. Robot., Autom. Mechatronics*, Qingdao, China, Sep. 2011, pp. 166–171.

[26] D. J. Todd, *Walking Machines: An Introduction to Legged Robots*. London, UK: Kogan Page, 2013.

[27] S. Peng, C. P. Lam, and G. R. Cole, "A biologically inspired four legged walking robot," in *Proc. IEEE Int. Conf. Robot. Autom.*, Taipei, Taiwan, Sep. 2003, pp. 2024–2030.

[28] Y. Sakagami, R. Watanabe, C. Aoyama, S. Matsunaga, N. Higaki, and K. Fujimura, "The intelligent ASIMO: System overview and integration," in *Proc. IEEE/RSJ Int. Conf. Intell. Robots Syst.*, Lausanne, Switzerland, Oct. 2002, pp. 2478–2483.

[29] W. Ilg, K. Berns, H. Jedele, J. Albiez, R. Dillmann, M. Fischer, H. Witte, J. Biltzinger, R. Lehmann, and N. Schilling, "BISAM: From small mammals to

a four legged walking machine," in *Proc. From Animals to Animates: 5th Int. Conf. Society for Adaptive Behaviour*, Zrich, Switzerland, 1998, pp. 400–407.

[30] A. Schneider, J. Paskarbeit, M. Schäffersmann, and J. Schmitz, "Biomechatronics for embodied intelligence of an insectoid robot," in *Proc. 4th Int. Conf. Intell. Robot. Appl.*, Aachen, Germany, Dec. 2011, pp. 1–11.

[31] J. Buchli, J. Pratt, N. Roy, M. P. Murphy, A. Saunders, C. Moreira, A. A. Rizzi, and M. Raibert, "The LittleDog robot," *Int. J. Robot. Res.*, vol. 30, no. 2, pp. 145–149, 2011.

[32] M. Bajracharya, J. Ma, M. Malchano, A. Perkins, A. A. Rizzi, and L. Matthies, "High fidelity day/night stereo mapping with vegetation and negative obstacle detection for vision-in-the-loop walking," in *Proc. IEEE/RSJ Int. Conf. Intell. Robots Syst.*, Tokyo, Japan, Nov. 2013, pp. 3663–3670.

[33] H. Kimura, Y. Fukuoka, and A. H. Cohen, "Biologically inspired adaptive walking of a quadruped robot," *Phil. Trans. R. Soc. A*, vol. 365, no. 1850, pp. 153–170, 2007.

[34] M. Raibert, K. Blankespoor, G. Nelson, R. Playter, and T. B. Team, "Bigdog, the rough-terrain quadruped robot," in *Proc. 17th World Congr.*, Seoul, Korea, Jul. 2008, pp. 10 822–10 825.

[35] X. Zhou and S. Bi, "A survey of bio-inspired compliant legged robot designs," *Bioinspir. Biomim.*, vol. 7, no. 4, pp. 1–20, 2012.

[36] S. P. Singh and K. J. Waldron, "Attitude estimation for dynamic legged locomotion using range and inertial sensors," in *Proc. IEEE Int. Conf. Robot. Autom.*, Barcelona, Spain, Apr. 2005, pp. 1663–1668.

[37] B. Brown and G. Zeglin, "The bow leg hopping robot," in *Proc. IEEE Int. Conf. Robot. Autom.*, Leuven, Belgium, May. 1998, pp. 781–786.

[38] E. Moore, D. Campbell, F. Grimminger, and M. Buehler, "Reliable stair climbing in the simple hexapod 'RHex'," in *Proc. IEEE Int. Conf. Robot. Autom.*, Washington, USA, May. 2002, pp. 2222–2227.

[39] H.-W. Park, K. Sreenath, A. Ramezani, and J. W. Grizzle, "Switching control design for accommodating large step-down disturbances in bipedal robot walking," in *Proc. IEEE Int. Conf. Robot. Autom.*, Minneapolis, USA, May. 2012, pp. 45–50.

[40] P. Birkmeyer, K. Peterson, and R. S. Fearing, "Dash: A dynamic 16 g hexapedal robot," in *Proc. IEEE/RSJ Int. Conf. Intell. Robots Syst.*, St. Louis, USA, Oct. 2009, pp. 2683–2689.

[41] A. T. Baisch, C. Heimlich, M. Karpelson, and R. J. Wood, "Hamr3: An autonomous 1.7 g ambulatory robot," in *Proc. IEEE/RSJ Int. Conf. Intell. Robots Syst.*, San Francisco, USA, Sep. 2011, pp. 5073–5079.

[42] A. M. Dollar, C. R. Wagner, and R. D. Howe, "Embedded sensors for biomimetic robotics via shape deposition manufacturing," in *Proc. 1st IEEE/RAS-EMBS Int. Conf. Biomed. Robot. Biomechatron.*, Pisa, Italy, Feb. 2006, pp. 763–768.

[43] M. Buehler, R. Battaglia, A. Cocosco, G. Hawker, J. Sarkis, and K. Yamazaki, "Scout: A simple quadruped that walks, climbs, and runs," in *Proc. IEEE Int. Conf. Robot. Autom.*, Leuven, Belgium, May. 1998, pp. 1707–1712.

[44] S. Hirose, "Some considerations on a feasible walking mechanism as a terrain vehicle," in *Proc. 3rd RoManSy Symp.*, Udine, Italy, Sep. 1978, pp. 357–375.

[45] S. Hirose and Y. Umetani, "The basic motion regulation system for a quadruped walking vehicle," in *Design Engineering Tech. Conf. ASME*, Los Angeles, USA, Sep. 1980, paper 80-DET-34, pp. 1–6.

[46] K. Arikawa and S. Hirose, "Development of quadruped walking robot TITAN-VIII," in *Proc. IEEE/RSJ Int. Conf. Intell. Robots Syst.*, Osaka, Japan, Nov. 1996, pp. 208–214.

[47] S. Kagami, K. Okada, M. Kabasawa, Y. Matsumoto, A. Konno, M. Inaba, and H. Inoue, "A vision-based legged robot as a research platform," in *Proc. IEEE/RSJ Int. Conf. Intell. Robots Syst.*, Victoria, Canada, Oct. 1998, pp. 235–240.

[48] H.-W. Park, M. Y. Chuah, and S. Kim, "Quadruped bounding control with variable duty cycle via vertical impulse scaling," in *Proc. IEEE/RSJ Int. Conf. Intell. Robots Syst.*, Chicago, USA, Sep. 2014, pp. 3245–3252.

[49] N. Kohl and P. Stone, "Policy gradient reinforcement learning for fast quadrupedal locomotion," in *Proc. IEEE Int. Conf. Robot. Autom.*, New Orleans, USA, Apr. 2004, pp. 2619–2624.

[50] S. Seok, A. Wang, M. Y. M. Chuah, D. J. Hyun, J. Lee, D. M. Otten, J. H. Lang, and S. Kim, "Design principles for energy-efficient legged locomotion and implementation on the MIT Cheetah robot," *IEEE/ASME Trans. Mechatronics*, vol. 20, no. 3, pp. 1117–1129, 2015.

[51] M. W. Spong, S. Hutchinson, and M. Vidyasagar, *Robot Modeling and Control*. New York, NY, USA: Wiley, 2006.

[52] R. B. McGhee and A. A. Frank, "On the stability properties of quadruped creeping gaits," *Mathematical Biosciences*, vol. 3, no. 3, pp. 331–351, 1968.

[53] M. Hildebrand, "Symmetrical gaits of horses," *Science*, vol. 150, no. 3697, pp. 701–708, 1965.

[54] W. Xi, Y. Yesilevskiy, and C. D. Remy, "Selecting gaits for economical locomotion of legged robots," *Int. J. Robot. Res.*, vol. 35, no. 9, pp. 1140–1154, 2016.

[55] M. Hutter, C. Gehring, D. Jud, A. Lauber, and C. D. Bellicoso, "Anymal–a highly mobile and dynamic quadrupedal robot," in *Proc. IEEE/RSJ Int. Conf. Intell. Robots Syst.*, Daejeon, Korea, Oct. 2016, pp. 38–44.